Tectonics

RESEARCH ARTICLE
10.1029/2022TC007244

Key Points:

- Anisotropy of Magnetic Susceptibility (AMS) and structural analysis constrained the tectonic evolution of the Rio do Peixe Basin
- The N-S to NNE-SSW extension is associated with the syn-rift phase I. The NW-SE extension occurred during syn-rift phase II
- The stretching direction gradually shifted from NNE-SSW to NW-SE due to clockwise rotation of the main stress fields associated to Pangea Breakup

Correspondence to:
M. A. Nicchio,
matheus.amadornicchio@unipr.it

Citation:
Nicchio, M. A., Balsamo, F., Cifelli, F., Nogueira, F. C. C., Aldega, L., Bezerra, F. H. R., et al. (2022). An integrated structural and magnetic fabric study to constrain the progressive extensional tectonics of the Rio do Peixe Basin, Brazil. *Tectonics*, *41*, e2022TC007244. https://doi.org/10.1029/2022TC007244

Received 2 FEB 2022
Accepted 26 SEP 2022

Author Contributions:
Conceptualization: M. A. Nicchio, F. Balsamo, F. C. C. Nogueira, F. H. R. Bezerra, D. L. Vasconcelos
Data curation: M. A. Nicchio
Formal analysis: M. A. Nicchio, F. Balsamo, F. Cifelli, L. Aldega
Funding acquisition: F. C. C. Nogueira, J. A. B. Souza
Investigation: M. A. Nicchio, F. Balsamo, F. Cifelli, D. L. Vasconcelos
Methodology: M. A. Nicchio, F. Balsamo, F. Cifelli, L. Aldega
Project Administration: F. C. C. Nogueira, J. A. B. Souza
Resources: F. C. C. Nogueira, J. A. B. Souza
Supervision: F. Balsamo

An Integrated Structural and Magnetic Fabric Study to Constrain the Progressive Extensional Tectonics of the Rio do Peixe Basin, Brazil

M. A. Nicchio[1], F. Balsamo[1], F. Cifelli[2], F. C. C. Nogueira[3], L. Aldega[4], F. H. R. Bezerra[5], D. L. Vasconcelos[3], and J. A. B. Souza[6]

[1]Department of Chemistry, Life Science and Environmental Sustainability, University of Parma, Parma, Italy, [2]Dipartimento di Scienze, Università Roma TRE, Rome, Italy, [3]Laboratório de Pesquisa Em Exploração Petrolífera, Departamento de Engenharia Do Petróleo, Universidade Federal de Campina Grande, Campina Grande, Brazil, [4]Dipartimento di Scienze dela Terra, Sapienza Università di Roma, Rome, Italy, [5]Universidade Federal Do Rio Grande Do Norte, Campus Universitário, Natal, Brazil, [6]Petrobras, Rio de Janeiro, Brazil

Abstract We constrained the tectonic evolution of the intracratonic Cretaceous Rio do Peixe Basin (RPB) in NE Brazil, combining structural and Anisotropy of Magnetic Susceptibility (AMS) data. We analyzed the structural features of four sites along two major faults bordering the basin, the NE-striking Portalegre Fault and the E-W-striking Malta Fault. AMS data from 42 sites in the syn-rift sandstone suggest two stretching directions driving the opening of the RPB. The early syn-rift phase I resulted from N-S to NNE-SSW stretching direction with vertical σ1, producing normal fault displacement along the E-W-striking Malta Fault and right-lateral transtension along the NE-striking Portalegre Fault, Sítio Saguí and Lagoa do Forno faults. The syn-rift phase II resulted from NW-SE stretching direction with vertical σ1, causing normal displacement on NE-striking major faults and left-lateral transtension on E-W-striking major faults. Additionally, the NW-SE extension was responsible for forming NE-striking extensional faults and deformation bands in sedimentary units. The RPB developed due to the intraplate deformation of the Borborema Province during the early stage of the Pangea Breakup and recorded two stretching directions that gradually shifted from NNE-SSW to NW-SE as a consequence of the South America clockwise rotation. The extensional stress orthogonal to the main E-W-striking and NE-striking Precambrian shear zones facilitated the opening and evolution of the RPB.

1. Introduction

Anisotropy of Magnetic Susceptibility (AMS) has been widely used as a proxy for the tectonic interpretation of sedimentary basins (Borradaile & Jackson, 2004; Faccenna et al., 2002; García-Lasanta et al., 2018; Porreca & Mattei, 2012). As the magnetic fabric is concordant with the gross petrofabric of the rock (Borradaile, 1988), it represents a powerful tool for tectonic reconstructions, even in rocks at a low grade of deformation or in zones where deformation is not visible (Cifelli et al., 2004; Schwehr & Tauxe, 2003).

Pangea Breakup is one of the most important events in the tectonic history of the Earth. This event started at ~145 Ma and determined the present-day continent configuration (Heine et al., 2013; Moulin et al., 2010; Peace et al., 2020). Its understanding is crucial as one of its main results is the opening of the Atlantic Ocean. The event was responsible for the rifting events that resulted in several sedimentary basins in South and North America, Africa and Europe, not only at the coast but also in intracontinental settings (Frizon De Lamotte et al., 2015; Heine et al., 2013; Moulin et al., 2010; Peace et al., 2020). Thus, the tectonic study of the syn-rift intracontinental basins is an excellent proxy for a better understanding of the Pangea Breakup event (Frizon De Lamotte et al., 2015). In the Borborema Province, northeastern Brazil, the initial stress responsible for the Pangea Breakup is recorded as dykes (Matos et al., 2021) and intracontinental syn-rift sedimentary basins (Celestino et al., 2020; Gomes et al., 2018).

In this study, we use the Rio do Peixe Basin (RPB) as a case study to contribute to understanding the Pangea Breakup event and its effects in the Borborema Province. In the case of the RPB, interpreting the extension directions responsible for the opening of the basin has been very challenging, mainly due to the lack of structural field information, in particular from its central regions, where apparently undeformed fine sandstones and shales are exposed (Françolin et al., 1994; Sénant & Popoff, 1991). When detected, intrabasinal deformation

Validation: M. A. Nicchio, F. Balsamo, F. Cifelli, F. C. C. Nogueira, L. Aldega, F. H. R. Bezerra
Writing – original draft: M. A. Nicchio, F. Balsamo
Writing – review & editing: M. A. Nicchio, F. Balsamo, F. Cifelli, F. C. C. Nogueira, L. Aldega, F. H. R. Bezerra, D. L. Vasconcelos

occurs as deformation bands mainly developed on coarse sandstones, while a complex network of deformation bands and minor faults are localized in the proximity of major basin-boundary faults (Araujo et al., 2018; Nicchio et al., 2018; Nogueira et al., 2015, 2021; Pontes et al., 2019; Souza et al., 2021; Silva et al., 2022; Torabi et al., 2021). The lack of clear kinematic features, typical of deformation bands in porous sandstone, makes the interpretation of the displacement direction and paleostress field evolution within the sedimentary units very complex.

Based on structural data, seismic interpretations, and potential data, previous studies discussed the Cretaceous syn-rift (Sénant & Popoff, 1991; Françolin et al., 1994; de Castro et al., 2007; Marques et al., 2014; Gomes et al., 2018; Celestino et al., 2020) and the Cenozoic post-rift tectonic inversion (Marques et al., 2014; Nogueira et al., 2015; Vasconcelos et al., 2021) of the intracontinental basins of Northeast Brazil during the Pangea Breakup. Several works tried to constrain the evolution of intraplate tectonic activity responsible for the opening of intracontinental sedimentary basins in the Borborema Province using the RPB as the most representative case study (e.g., De Castro et al., 2007; Marques et al., 2014; Nogueira et al., 2015). However, there is still no consensus about the acting stress responsible for the opening of the RPB, and, consequently, other intracontinental basins in NE Brazil. While some works suggest a model of compression resulting on N-S extension (Szatmari et al., 1987) or local NW-SE extension in pull-apart basins (Françolin et al., 1994), others propose a simple N-S extension with vertical maximum stress during the Cretaceous syn-rift stage (Sénant & Popoff, 1991). Such information is of paramount importance to better constrain the tectonic evolution of Northeast Brazil during the Pangea Breakup.

In this study, we present a new interpretation of the development and tectonic evolution of the RPB, mainly focusing on the stretching directions along the whole basin during the syn-rift stage. We used AMS and structural data collected on both main border faults and intrabasin domains. Results suggest that two orthogonal stretching directions are responsible for the Pangea Breakup, thus opening new research lines in intracontinental siliciclastics sediments of the Borborema Province in northeast Brazil.

2. Geological Settings

The Rio do Peixe (RPB) is an intracontinental basin bounded by Precambrian shear zones in the Borborema Province, northeast Brazil (Figure 1a). The RPB is one of the most important sedimentary basins in the region, tectonically correlated with other basins in northeast Brazil (Matos, 1992). The RPB is composed of three sub-basins, from W to E, named Brejo das Freiras (BFSB), Sousa (SSB), and Pombal (Figures 1a and 1B). All sub-basins present major border faults opposed to flexural borders (Nogueira et al., 2004; Sénant & Popoff, 1991). The sub-basins are elongated following the trend of their border faults: NE-SW Portalegre Fault (Brejo das Freiras), E-W Malta Fault (Sousa) and NE-SW Rio Piranhas Fault (Pombal). Two main depocenters were identified in the basin by gravimetry (de Castro et al., 2007; Nogueira et al., 2004) and seismic data (Rapozo et al., 2021; Vasconcelos et al., 2021). In the BFSB, the depocenter is localized in the southern zone of the Portalegre Fault and follows the fault trend. In the SSB, the depocenter is aligned along the Malta Fault with deeper portions at the inflection zones between the NE-trending faults (Sítio Saguí and Lagoa do Forno) and the Malta Fault (Figure 1b).

The RPB presents a tectonic evolution characterized by syn-rift normal faulting and post-rift transpression (Nogueira et al., 2015; Vasconcelos et al., 2021). The opening of the basin is related to the brittle reactivation of the E-W-striking Patos and NE-striking Portalegre ductile shear zones (Figure 1a), branches of the major right-lateral Transbrasiliano lineament, formed as a result of the West Gondwana Orogen (~600 Ma) (Oriolo et al., 2017). This reactivation led to the development of the E-W-striking Malta Fault at the southern border of the SSB and the NE-striking Portalegre Fault at the eastern border of the BFSB (Françolin et al., 1994; Sénant & Popoff, 1991) (Figure 1b). The RPB presents Devonian pre-rift units (Lourenço et al., 2021; Rapozo et al., 2021; Vasconcelos et al., 2021) and Cretaceous rift units that span from the early (145 Ma) to late Cretaceous (125 Ma) (Lima & Coelho, 1987; Arai, 2006; Sousa et al., 2018). It suggests that the Cretaceous rifting of the basin is related to intracontinental deformation during the initial opening of the Atlantic Ocean (Matos, 1992).

The extensional tectonics of the basin is still debated, as distinct interpretations have been proposed. Szatmari et al. (1987) interpreted that the basin was formed due to N-S-oriented extension. According to the authors, during the initial stage of the opening of the Atlantic Ocean, the clockwise rotation of the South American continent

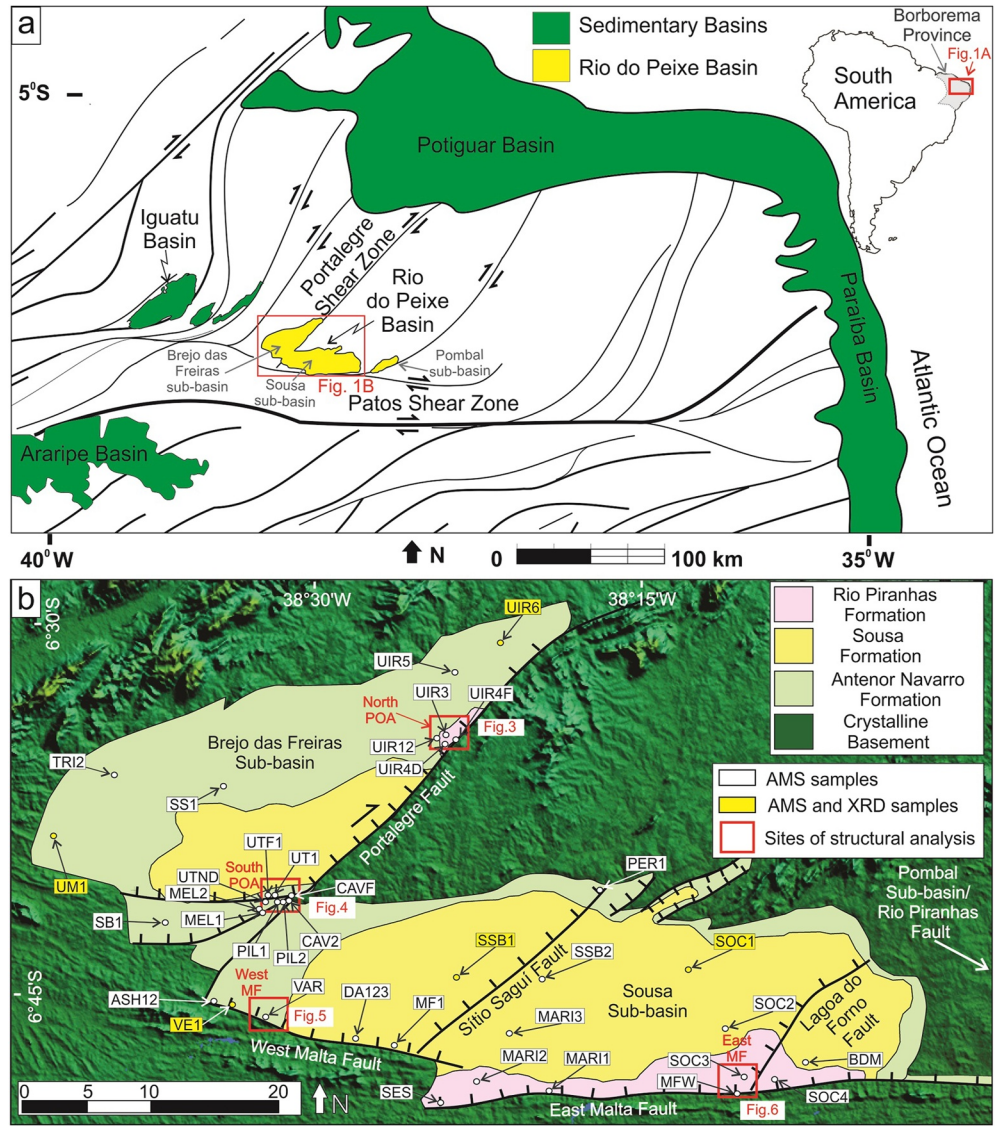

Figure 1. (a) Location of the Rio do Peixe Basin in a simplified tectonic framework of northeastern Brazil (modified from Nogueira et al., 2015). (b) Geological map of the Rio do Peixe Basin with major structures (modified from Nogueira et al., 2021). Red boxes indicate the studied outcrops for structural analysis. White dots indicate the location of AMS (Anisotropy of Magnetic Susceptibility) sampling sites. White and yellow boxes indicate the name of the sampling locality for AMS analysis and the name of the sample. Yellow boxes indicate the samples analyzed with X-ray diffraction (XRD).

would have pressed the northeastern region of Brazil against the African continent, resulting in an E-W-oriented compression and a N-S-oriented extension. Following a similar interpretation, Françolin et al. (1994) suggested that the initial opening of the RPB is marked by NW-SE-oriented extension as a result of ENE-WSW-oriented compression, thus generating a left-lateral wrenching. On the other hand, Sénant and Popoff (1991) proposed that the N-S-oriented extension with vertical σ_1 might have been the initial stretching direction of the basin.

The post-rift stage of RPB was marked by tectonic inversion, identified through reverse reactivated border faults (Nogueira et al., 2015) and inverted deep normal faults within the basin (Vasconcelos et al., 2021). During this inversion stage, an E-W-oriented compression was responsible for reactivating the rift faults under horizontal compression (Nogueira et al., 2015; Vasconcelos et al., 2021).

Three main Cretaceous synchronous and heterolytic rift siliciclastic formations occur in the RPB (Lima & Coelho, 1987; Arai, 2006; Sousa et al., 2018). The Antenor Navarro Formation is a fluvial deposit composed of

braided rivers, where basal trough cross-bedding conglomerates are predominant (Françolin et al., 1994). They occur as metric-scale channel deposits, where the conglomerates are overlapped by medium and fine grained sandstones on fining upwards deposits. The Sousa Formation is composed of fine-grained deposits, with the predominance of mudstones, muddy sandstones, and marls (Sénant & Popoff, 1991). The Sousa Formation is composed of meandering rivers interspersed with flood plains. The Rio Piranhas Formation is composed of coarse conglomerates that interfinger with sandstones and siltstones. Its occurrence is restricted to the border faults and is interpreted as alluvial fan deposits, which resulted from the fault evolution during the opening of the basin (Françolin et al., 1994; Sénant & Popoff, 1991). Based on X-ray diffraction analysis of clay minerals of outcrop samples, Maciel et al. (2018) suggested that the three formations experienced a maximum burial depth of <1–2 km.

3. Methods

Field data consist of structural and paleocurrent analysis. The structural analysis was performed on four areas (red boxes in Figure 1b) along the main fault zones. We collected structural data from faults, open fractures, and deformation bands along the northern and southern areas of the Portalegre Fault, and the eastern and western areas of the Malta Fault (Figure 1b). In the exposures close to the bordering fault, we compared structural data from the crystalline basement (35 fault planes and 73 fractures) with rift units deformation of the major fault damage zone (19 fault planes and 44 deformation bands). As only a few striae and kinematic indicators were identified on the border fault, we used joints to infer the extensional direction on the crystalline basement, since joint directions strike perpendicular to the minimum principal stress (σ_3) (Dyer, 1988). Also, we measured a total of 88 paleocurrents from 15 outcrops, considering the average cross-through bedding and ripple directions in each site as indicative of paleocurrent direction.

We also performed AMS analysis, a non-destructive method that allows characterizing deposition and deformation patterns of sedimentary deposits. AMS is defined by a symmetric second rank tensor and represented geometrically by an ellipsoid with principal axes K_1, K_2, K_3. Several parameters have been defined both for quantifying the magnitude of anisotropy and for defining the shape of the ellipsoid (Table 2; Hrouda, 1982). The T-shape parameter varies from +1 (perfectly oblate ellipsoid, $K_1 = K_2 > K_3$) to −1 (perfectly prolate ellipsoid, $K_1 > K_2 = K_3$), while a value of 0 corresponds to a triaxial ellipsoid. The magnetic lineation L (K_1/K_2) is defined by the orientation of K_1, while the magnetic foliation F (K_2/K_3) is defined as the plane perpendicular to K_3. The parameter P_j expresses the anisotropy degree (Jelinek, 1981). The mean magnetic susceptibility ($K_{mean} = (K_1 + K_2 + K_3)/3$) gives a relative estimation of the amount of magnetic minerals in the sample (Borradaile, 1988; Rochette et al., 1992).

In undeformed sedimentary units, the magnetic susceptibility ellipsoid is generally oblate with the foliation plane subparallel to bedding; this fabric is attributed to depositional and/or compaction processes (Hamilton & Rees, 1970; Lee et al., 1990; Paterson et al., 1995). If sediments undergo tectonic deformation, an AMS sub-fabric progressively develops, modifying the primary magnetic fabric according to the nature and extent of deformation (e.g., Borradaile & Tarling, 1981). Particularly in extensional basins, the magnetic lineation usually coincides with the maximum stretching direction, which is orthogonal to the main normal faults and generally aligned with the dip direction of bedding (Cifelli et al., 2005; Mattei et al., 1997).

In this study, we collected a minimum of four cylindrical cores with a battery-powered driller equipped with a cooling water pump in 42 sites (Figure 1b). When possible, the sampling was performed on clay-rich rocks. Extracted cores (2.5 cm in diameter and 3–15 cm long) were oriented in situ by a magnetic compass. All oriented samples were sliced into standard cylindrical specimens of 2.5 cm in diameter and 2.1 in height. For each site, a minimum of 9 specimens were measured to obtain the site mean magnetic fabric orientation (Table 1). Measurements were carried out on a total of 531 samples, being 316 on the SSB and 225 on the BFSB.

The low field magnetic susceptibility (k) was measured in the laboratory of Paleomagnetism at Roma Tre University. We used the KLY-3 from the Kappa bridge equipment. For data processing, we used the software Anisoft 4.2 (Chadima & Jelinek, 2009), applying Jelinek's statistics (Jelinek, 1981) to evaluate and validate the acquired anisotropy degree and shape parameter data. As primary structures of rocks might influence the AMS fabric (Borradaile, 1988; Rochette et al., 1992), we compared the acquired magnetic fabric of each sample with the dip direction of bedding and paleocurrent of each site to constrain better the origin of the magnetic fabric, either

Table 1
Site Mean AMS Data

Location	Site	Coord_X	Coord_Y	Lithology	N	K_{mean}	T	L	F	P_j	B0	K_1 (D/I)	K3 (D/I)	Paleo-current (AZ)
BFSB	ASH1-2	545979	9251331	Sandstone	20	3.52E−05	0.456 (0.261)	1.009 (0.0013)	1.025 (0.0013)	1.036 (0.028)	n	132/13	292/75	
BFSB	CAVF	552151	9259450	Sandstone	28	9.48E−05	0.457 (1.181)	1.007 (0.004)	1.02 (0.005)	1.028 (0.008)	350/35	128/08	007/75	310
BFSB	CAV2	552091	9259418	Sandstone	14	4.83E−05	0.641 (0.242)	1.006 (0.008)	1.029 (0.017)	1.038 (0.015)	350/35	179/23	017/65	310
BFSB	MEL2	549894	9258471	Sandstone	10	3.30E−05	0.796 (0.220)	1.003 (0.005)	1.03 (0.007)	1.037 (0.006)	334/14	306/29	134/61	
BFSB	SB1	542990	9258018	Siltstone	10	2.59E−05	−0.611 (0.366)	1.017 (0.007)	1.004 (0.008)	1.023 (0.010)	225/31	301/11	196/54	
BFSB	SS1	547456	9268415	Sandstone	10	5.62E−05	0.546 (0.350)	1.006 (0.022)	1.021 (0.006)	1.029 (0.025)	180/10	136/10	340/79	124
BFSB	TRI2	538532	9269211	Sandstone	10	5.57E−05	0.057 (0.306)	1.01 (0.004)	1.011 (0.011)	1.021 (0.013)	159/11	214/18	012/09	
BFSB	UIR1-2	564426	9271895	Sandstone	20	6.53E−05	0.497 (0.395)	1.006 (0.006)	1.019 (0.015)	1.027 (0.018)	283/15	128/07	240/71	
BFSB	UIR3	564413	9271278	Sandstone	10	5.64E−03	0.94 (0.063)	1.002 (0.003)	1.054 (0.012)	1.063 (0.015)	232/15	293/01	030/82	
BFSB	UIR5	564856	9275867	Sandstone	10	8.04E−05	0.649 (0.249)	1.005 (0.003)	1.026 (0.013)	1.033 (0.015)	174/13	179/09	359/80	150
BFSB	UIR6	569049	9278946	Sandstone	10	4.92E−05	0.556 (0.434)	1.007 (0.005)	1.023 (0.016)	1.031 (0.017)	210/06	264/04	016/80	
BFSB	UM1	533058	9264597	Sandstone	9	5.40E−05	0.028 (0.297)	1.003 (0.004)	1.003 (0.002)	1.006 (0.004)	118/20	011/04	104/39	
SSB	MARI1	572331	9244220	Sandstone	12	1.55E−04	0.415 (0.490)	1.012 (0.027)	1.03 (0.011)	1.044 (0.030)	040/59	317/26	210/32	
SSB	MARI2	566468	9244766	Sandstone	17	8.48E−05	0.836 (0.102)	1.004 (0.003)	1.044 (0.011)	1.054 (0.012)	145/04	144/06	339/83	165
SSB	MARI3	569189	9249537	Sandstone	13	1.42E−04	0.693 (0.199)	1.008 (0.005)	1.043 (0.010)	1.056 (0.010)	186/10	275/01	009/77	106
SSB	PER1	576328	9260129	Sandstone	10	8.50E−05	0.757 (0.190)	1.009 (0.009)	1.067 (0.012)	1.084 (0.015)	196/05	149/08	321/81	
SSB	SOC1	583168	9253770	Siltstone	10	1.41E−04	−0.347 (0.139)	1.005 (0.002)	1.002 (0.001)	1.008 (0.003)	179/13	336/82	075/01	
SSB	SOC2	586118	9248867	Siltstone	13	1.63E−04	0.878 (0.250)	1.001 (0.001)	1.012 (0.005)	1.014 (0.006)	200/09	267/07	051/81	230
SSB	SOC3	587844	9245717	Siltstone	16	9.83E−05	0.553 (0.411)	1.003 (0.003)	1.011 (0.005)	1.015 (0.005)	230/11	140/03	000/86	251
SSB	SOC4	590026	9245607	Siltstone	12	6.51E−05	0.368 (0.356)	1.006 (0.011)	1.014 (0.018)	1.02 (0.028)	200/11	202/01	102/87	250
SSB	SSB1	565095	9253257	Siltstone	10	9.30E−05	0.768 (0.231)	1.003 (0.003)	1.021 (0.004)	1.026 (0.005)	164/16	185/14	356/75	
SSB	SSB2	571914	9253105	Siltstone	10	9.69E−05	0.667 (0.336)	1.005 (0.005)	1.024 (0.012)	1.031 (0.012)	180/13	159/08	348/82	305
SSB	UT1	550813	9259755	Sandstone	11	7.67E−05	0.899 (0.363)	1.001 (0.005)	1.022 (0.006)	1.026 (0.006)	148/09	176/06	326/82	
SSB	UTF1	550882	9259832	Sandstone	11	9.46E−05	0.869 (0.116)	1.003 (0.003)	1.038 (0.005)	1.046 (0.006)	145/09	165/03	016/86	165

Table 1
Continued

Location	Site	Coord_X	Coord_Y	Lithology	N	K_{mean}	T	L	F	P_j	B0	K_1 (D/I)	K3 (D/I)	Paleo-current (AZ)
SSB	UTND	550791	9259479	Sandstone	11	3.29E−05	0.806 (0.179)	1.004 (0.006)	1.04 (0.007)	1.049 (0.008)	170/20	211/03	072/86	
SSB	BDM	592289	9246819	Sandstone	15	2.38E−04	0.792 (0.200)	1.003 (0.002)	1.027 (0.012)	1.033 (0.013)	126/17	036/02	286/84	45
NPOA	UIR4F	565152	9271812	Sandstone	15	9.74E−05	0.549 (0.253)	1.009 (0.005)	1.018 (0.004)	1.029 (0.006)	084/09	190/02	331/87	
NPOA	UIR4D	565109	9271817	Sandstone	10	1.28E−04	0.419 (0.188)	1.012 (0.006)	1.03 (0.009)	1.044 (0.014)	084/09	013/37	151/06	
SPOA	MEL1	550061	9258456	Sandstone	10	9.18E−05	0.033 (0.259)	1.009 (0.004)	1.009 (0.007)	1.018 (0.008)	334/14	021/03	286/65	
SPOA	PIL1	551706	9259424	Sandstone	17	5.32E−05	0.757 (0.226)	1.005 (0.004)	1.018 (0.004)	1.024 (0.006)	269/08	269/06	041/80	
SPOA	PIL2	551692	9259446	Sandstone	12	7.64E−05	0.34 (0.235)	1.011 (0.004)	1.023 (0.007)	1.035 (0.007)	269/08	038/01	270/88	
WMF	DA123	557342	9248477	Sandstone	34	4.80E−05	0.637 (0.295)	1.01 (0.005)	1.044 (0.020)	1.057 (0.022)	008/43	290/02	196/65	
WMF	MF1	560242	9247706	Sandstone	9	2.63E−05	−0.039 (0.263)	1.016 (0.006)	1.014 (0.006)	1.03 (0.007)	024/55	286/14	36/54	
WMF	VE1	546693	9250948	Sandstone	9	2.71E−05	0.546 (0.433)	1.011 (0.011)	1.037 (0.034)	1.051 (0.039)	030/24	151/22	023/56	
WMF	VAR1	550042	9249855	Sandstone	9	5.63E−05	−0.496 (0.391)	1.014 (0.013)	1.005 (0.013)	1.02 (0.017)	043/38	128/37	007/35	40
WMF	VAR2	549886	9249881	Sandstone	12	4.06E−05	−0.355 (0.307)	1.021 (0.004)	1.01 (0.014)	1.032 (0.015)	044/13	155/05	064/13	40
WMF	VAR3	549810	9250154	Sandstone	10	7.14E−05	−0.207 (0.373)	1.011 (0.008)	1.007 (0.025)	1.019 (0.030)	035/20	334/19	193/66	40
WMF	VAR2-F	549998	9249938	Sandstone	29	6.30E−05	−0.579 (0.363)	1.008 (0.007)	1.002 (0.005)	1.01 (0.009)	030/13	149/03	250/73	40
EMF	MFW	587346	9245273	Sandstone	12	1.25E−04	0.74 (0.077)	1.006 (0.002)	1.042 (0.007)	1.053 (0.009)	298/22	27/17	164/67	280
EMF	SES	564317	9243460	Sandstone	11	7.78E−05	0.397 (0.380)	1.003 (0.003)	1.007 (0.003)	1.01 (0.004)	089/39	196/09	074/73	

Note. BFSB = Brejo das Freiras sub-basin. SSB = Sousa sub-basin. NPOA = North Portalegre Fault. SPOA = South Portalegre Fault. WMF = West Malta Fault. EMF = East Malta Fault. N = Number of specimens measured. K_{mean} = Mean anisotropy of magnetic susceptibility in SI units ($K_{mean} = K_1 + K_2 + K_3$). T = Magnetic ellipsoid shape parameter (varies from −1 to 1, where negative values indicate prolate shape and positive values indicate oblate shape). L = Magnetic lineation (K_1/K_3). F = Magnetic foliation (K_2/K_3). P_j = Corrected anisotropy degree (Jelinek, 1981). B0 = bedding (in dip direction/dip). K_1 = maximum magnetic anisotropy direction (K_{max}). K_3 = minimum magnetic anisotropy direction (K_{min}). D = K azimuth; I = K inclination. AZ = azimuth.

sedimentary or due to tectonic deformation. To interpret the type of magnetic fabric of each sample, we used the stereonet interpretation methodology proposed by Lanza and Meloni (2006). We classified as sedimentary magnetic fabric samples that presented the K_1 distributed around the equatorial plane of the stereonet and/or distributed along the bedding orientation or grouped parallel to the paleocurrent direction. The tectonic magnetic fabric was identified in samples where the k1 was well grouped in a single direction, and not coinciding with the dip direction of bedding and paleocurrent. To better discriminate the tectonic magnetic fabrics present in the RPB, we used the software Daisy3® to perform frequency and Gaussian best fit analysis with smooth interval of 20% of K_1 direction of all samples interpreted as tectonically affected magnetic fabric (total of 384 samples).

Magnetic mineralogy analyses were carried out on selected samples from the Antenor Navarro and Sousa formations of the RPB. Eight hysteresis loops were measured with a Lakeshore 8604 VSM Magnetometer at the INGV

10.1029/2022TC007244

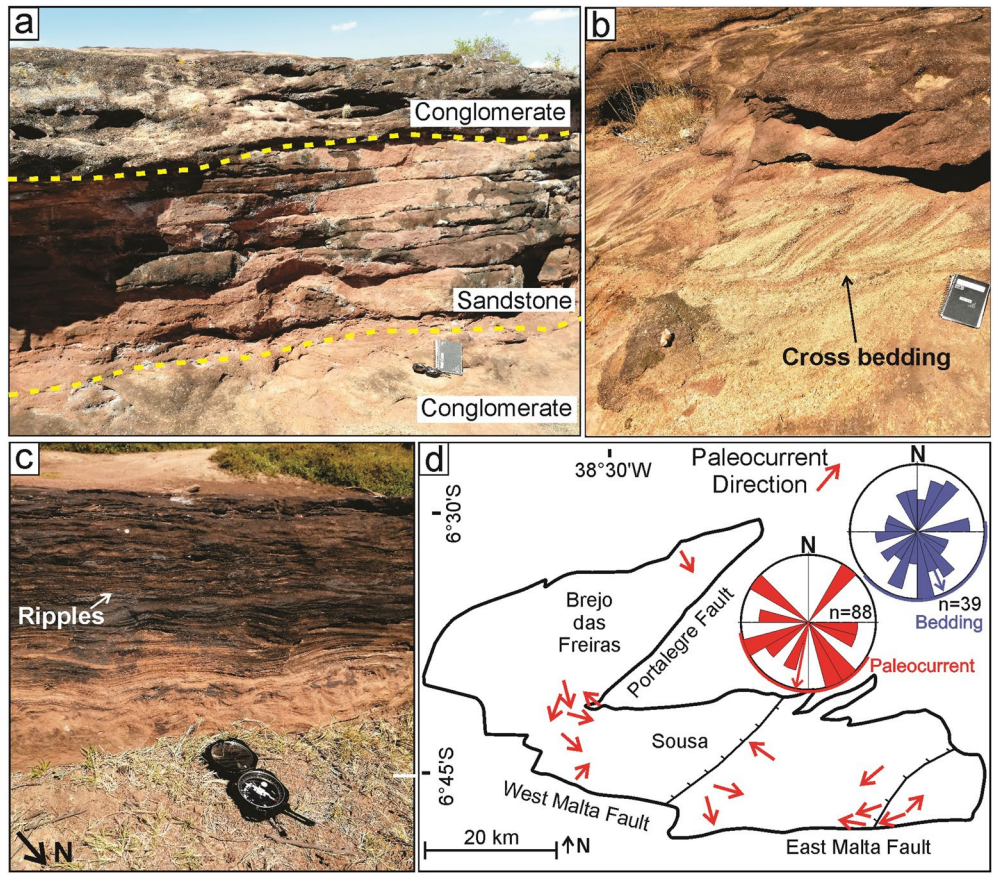

Figure 2. Host rock characteristics. (a) Section view of sandstone layers interbedded within two conglomerate layers (Antenor Navarro Fm.). (b) Detailed section view of conglomerate with cross-bedding (Antenor Navarro Fm.). (c) Detailed plan view of fine sandstone with ripple marks (Sousa Fm.). (d) Map view of paleocurrent direction (red arrows). Red stereogram indicates cumulative paleocurrent direction. Blue stereogram indicates the azimuth direction of the bedding in the outcrops.

in Rome. Moreover, eight thermomagnetic curves were measured using a CS-3 Agico Apparatus at the laboratory of Paleomagnetism at Roma Tre University.

4. Results

4.1. Paleocurrent Analysis of Syn-Rift Units

The Antenor Navarro Formation is composed of interbedding fine conglomerates and coarse sandstones (Figure 2a). The main facies of the Antenor Navarro Formation is composed of several decimetric to metric beds of fine conglomerates, which present features of high-energy river channels forming cross-through bedding (Figure 2b). Subparallel decimeter sandstone layers occur as lenses within the conglomerate beds (Figure 2a). The Sousa Formation is composed of laminated shale and clay-rich fine sandstones to siltstones with ripple marks (Figure 2c). The reconstructed paleocurrent directions are not homogeneous along the basin, and three main directions were observed: NE-SW, NW-SE, and E-W (Figure 2d). In the BFSB, the inner zones show paleocurrent directions toward SE and SSW, thus toward the Portalegre Fault. Close to the Portalegre Fault, the paleocurrent also follows the fault dip direction toward NW. In the SSB, different paleocurrent directions are observed. Near the Malta Fault, the paleocurrent direction occurs toward the border fault (SE and SW directions), subparallel to the border fault (toward W), and following the fault dip direction toward NE. In the inner portions of the SSB, the paleocurrent direction spans from SE, SW to NW direction (Figure 2d).

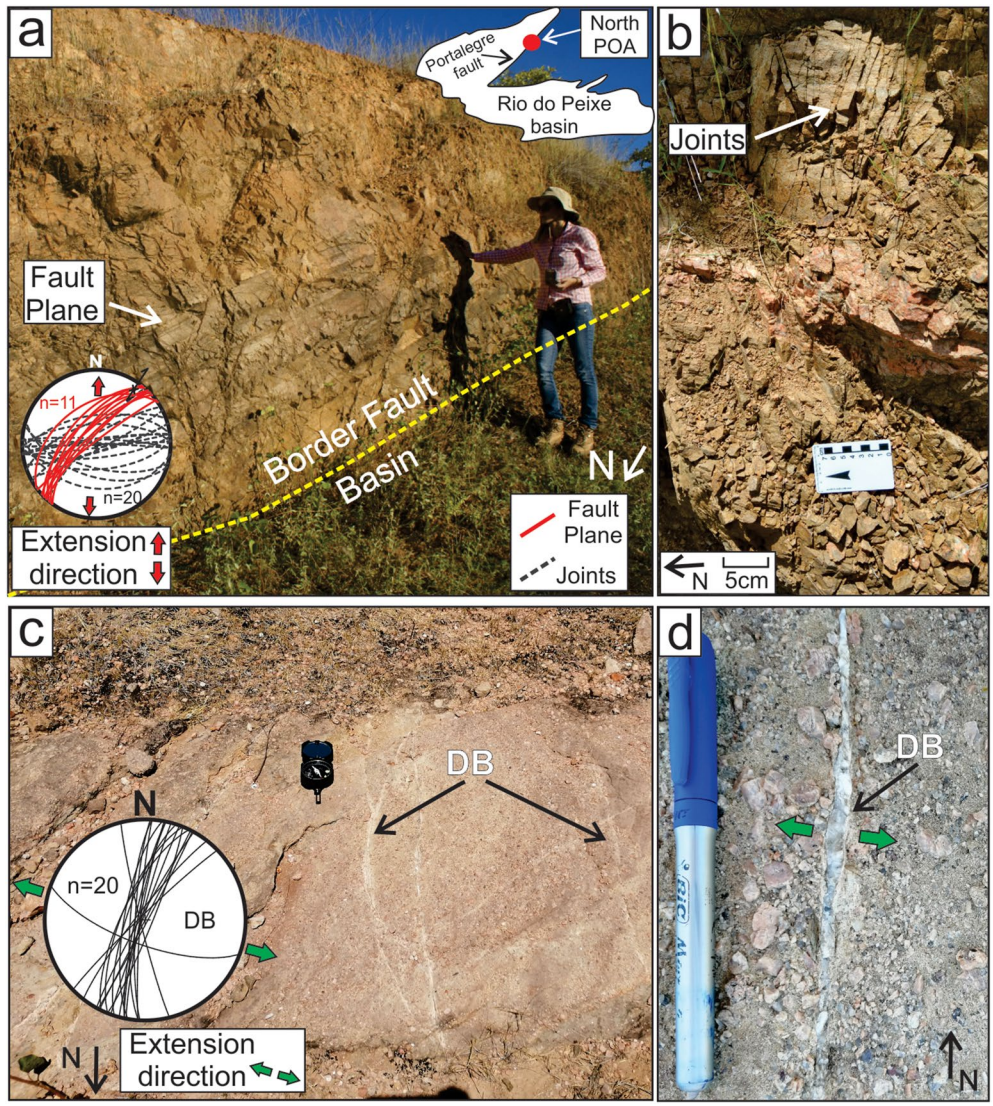

Figure 3. Outcrop view of the North Portalegre Fault: (a) NE-striking border fault in the crystalline basement with E-W-striking open joints compatible with right-lateral transtension. Red arrows indicate the extension direction. (b) Detail of E-W-striking open joints in fault footwall. (c) NNE-striking deformation bands in coarse sandstones of the Antenor Navarro Fm. close to the border fault. (d) Detail of NNE-striking deformation bands filled with quartz vein compatible with a WNW-ESE extension (green arrows). DB: deformation bands.

4.2. Structural Data

The border faults were analyzed in four distinct sites. Two sites were studied along the NE-striking Portalegre Fault: one in its northern zone (Figure 3) and one in its southern zone (Figure 4). The Portalegre Fault presents right-lateral transtensive movement with fault plane parallel to the Proterozoic ductile foliation of the Portalegre Shear Zone. In the E-W-striking Malta Fault, two sites were analyzed: one in its western zone (Figure 5) and one in its eastern zone (Figure 6). The Malta Fault presents normal displacement with fault plane parallel to the ductile foliation of the Patos Shear Zone.

4.2.1. North Portalegre Fault

The Portalegre Fault is well exposed in the northern region of the BFSB, where the crystalline basement is in contact with sedimentary units of the Antenor Navarro Formation. The fault strikes NE-SW and dips steeply toward NW (Figure 3a). The striae found on the main fault surface are sub-horizontal and indicate dextral movement. Several E-W trending joints are compatible with dextral movement (Figure 3b). Decimetric to metric

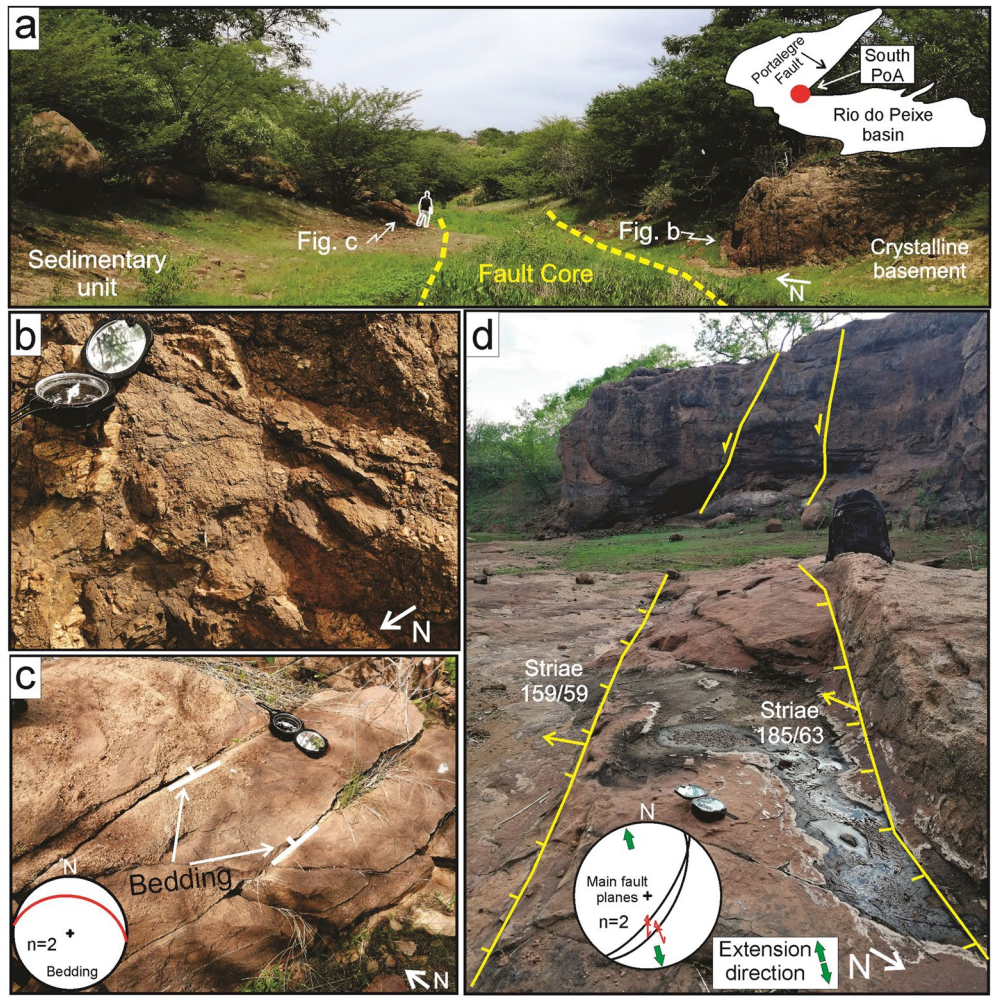

Figure 4. Outcrop view of South Portalegre Fault: (a) General view of the outcrop indicating the Portalegre Fault core separating the crystalline basement and sedimentary units of the Antenor Navarro Formation. (b) Detail of crystalline basement. (c) Detail of sedimentary units with beds dipping NNW. (d) Fault planes in sedimentary units antithetic to the major border fault. The faults strike NE with striae presenting low obliquity, indicating NW-SE-oriented extension (green arrows).

spaced NNE-striking deformation bands occur in conglomeratic sandstone of the damage zone (Figure 3c). The deformation bands are locally reopened and filled with quartz veins (Figure 3d).

4.2.2. South Portalegre Fault

In the Southern part of the Portalegre Fault, the crystalline basement is in contact with the Antenor Navarro Formation coarse sandstone (Figure 4a). The crystalline basement is intensely fractured and silicified, with border fault trending NE-SW (Figure 4b). Close to the fault, the sedimentary unit presents no visible deformation, preserving its original sedimentary features with bedding dipping toward NNW (Figure 4c). In the vicinity of the border fault core, minor NE-striking faults occur (Figure 4d). These minor faults that dip southward are antithetic to the Portalegre Fault and present striae with low obliquity to downdip.

4.2.3. West Malta Faults

On the western Malta Fault, the brecciated crystalline basement is in direct tectonic contact with the sedimentary unit of the Antenor Navarro Formation (Figure 5a). The main fault strikes E-W and dips 65°–70° northward (Figure 5a). Measured striae show normal displacement with low obliquity, indicating NNE-SSW-oriented extension. Also, several WNW-ESE- to E-W-striking joints in the footwall damage zone occur (Figure 5b), consistent with the almost pure normal fault kinematics and inferred NNE-SSW-oriented extension. E-W- to

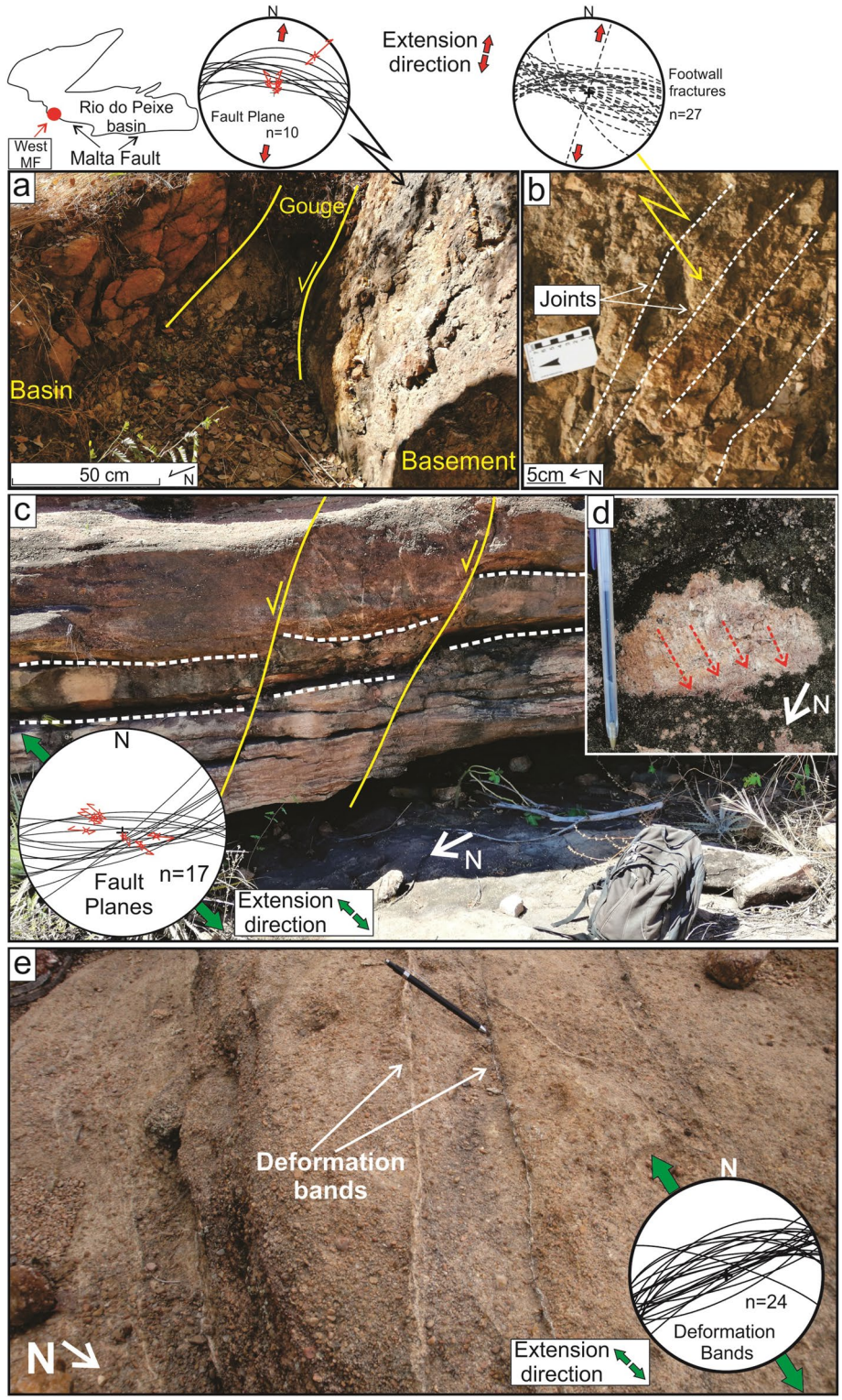

Figure 5. Outcrop view of West Malta Fault. (a) Contact zone between the crystalline basement and sedimentary units of the Antenor Navarro Formation. The border fault plane is WNW-ESE-striking with striae toward the north. Red arrows indicate the extension direction of the fault. (b) Detail of WNW-ESE-striking open joints in the fault footwall. (c) WSW-ENE left lateral transtensive faults with striae toward NW in the sedimentary unit. Green arrows indicate the extension direction. (d) Detail of fault striae indicating transtensive displacement toward NW. (e) WSW-ENE-striking deformation bands in the fault damage zone.

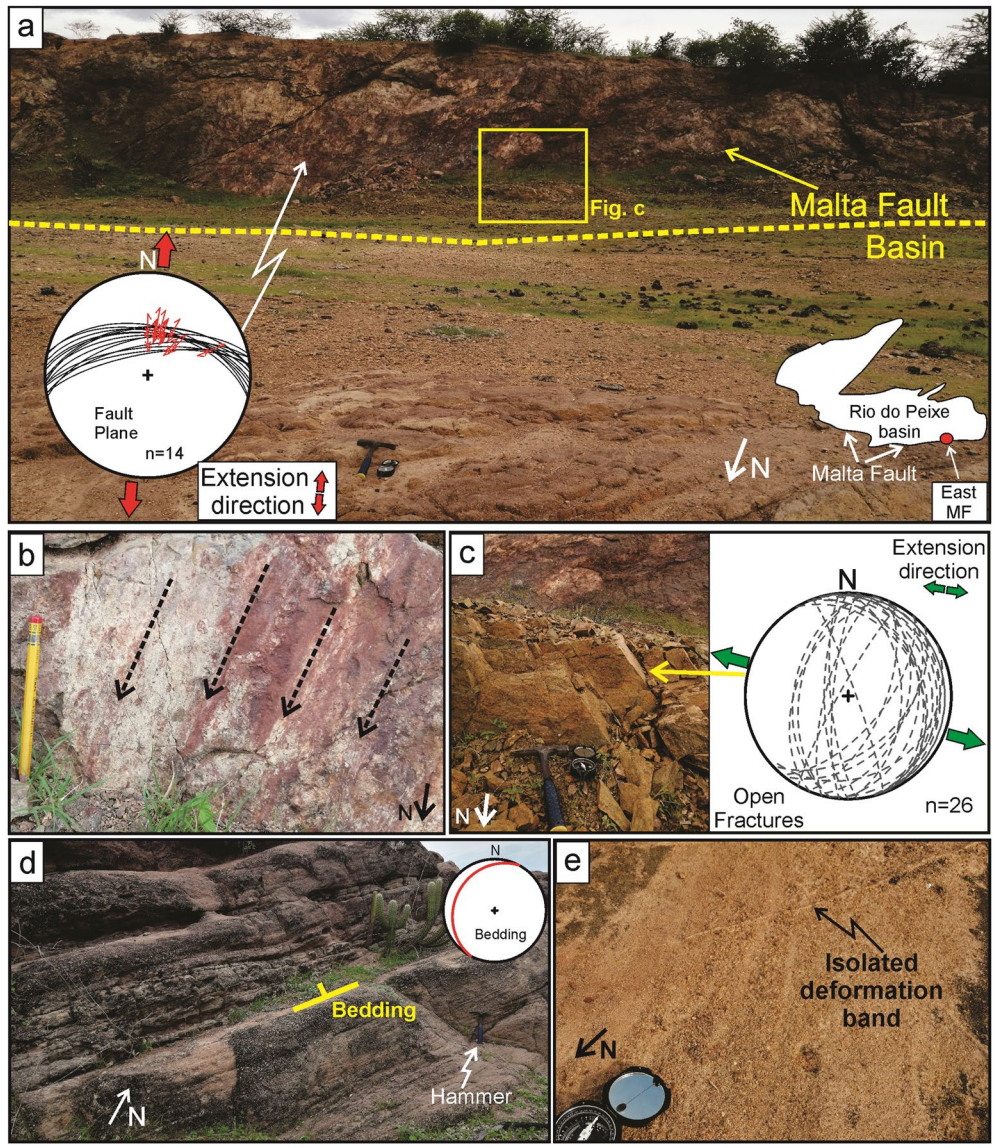

Figure 6. Outcrop view of East Malta Fault. (a) Major border E-W-striking fault scarp. Striae indicate downdip to right-lateral transtension (b) with a displacement of the hangingwall toward NNE. Red arrows indicate the extension direction. (c) Detail of NNE-striking open joints cross-cutting the mylonitic foliation in the major border fault. Green arrows indicate the extension direction. (d) Non-deformed coarse sandstone with bedding dipping NW. (e) Detail of isolated NE-striking deformation band indicating low deformation grade in the sedimentary unit.

ENE-WSW-striking minor faults, subparallel to the main border fault, occur in the sedimentary unit (Figures 5c and 5d). They exhibit left-lateral transtensive kinematics and decimetric displacement, indicating NW-SE-oriented extension. The hanging wall fault damage zone is also dominated by pervasive fault-parallel deformation bands (Figure 5e).

4.2.4. East Malta Fault

In the eastern part of the Malta Fault, the crystalline basement is in contact with the sedimentary unit of the Rio Piranhas Formation (Figure 6a). The border fault strikes E-W and dips 65°–70° to the north (Figure 6a). Striae on the main fault surface are downdip, indicating NNE-trending extension (Figure 6b). The main fault surface is cross-cut by NNE-striking joints (Figure 6c). The sedimentary unit exhibits a very low deformation grade, preserving its original sedimentary features close to the border fault (Figure 6d). Only a few mm-thick, NE-striking isolated deformation bands exhibit tens of meters spacing (Figure 6e).

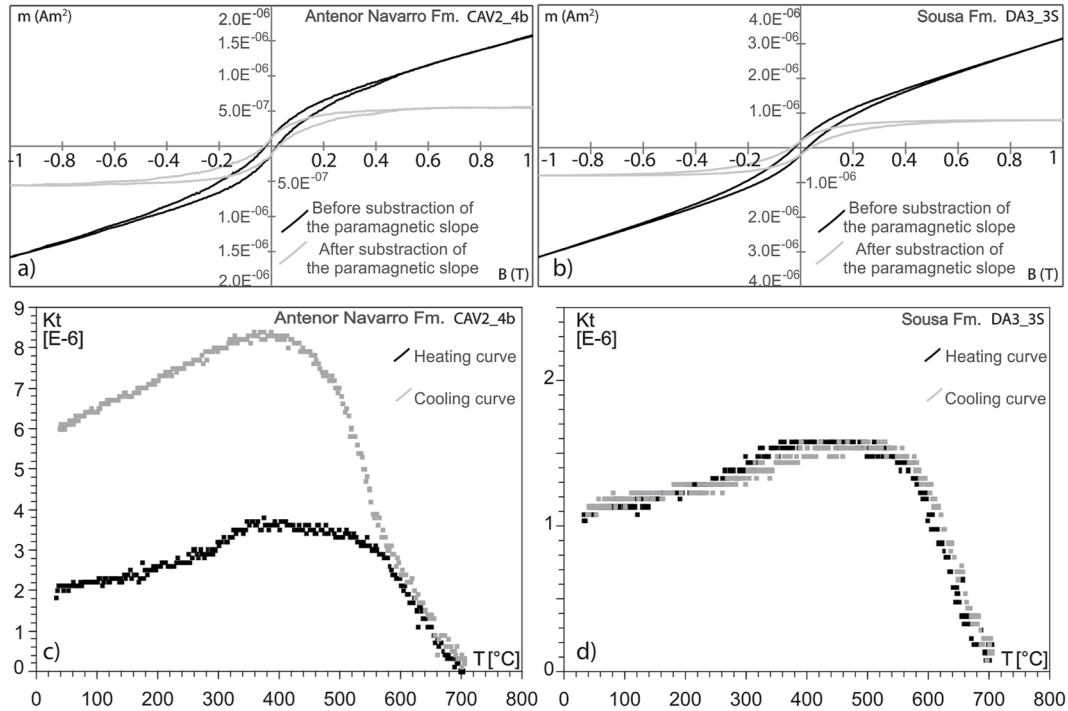

Figure 7. Hysteresis loops (a), (b) and thermomagnetic surveys (c),(d) for two representative specimens. The samples CAV2 and DA3 are representative samples of Antenor Navarro and Sousa formations, respectively.

4.3. AMS Data

4.3.1. Cumulative Statistical Analysis

The AMS data from samples collected within the RPB are reported in Table 1. Collectively, the AMS parameters present low anisotropy degrees with P_j values lower than 1.084 and K_{mean} lower than 5.4×10^{-03} SI, with a predominance of values between 10^{-5} and 10^{-4} SI (Table 1 and Figure 8e). The shape parameter of most samples from the Antenor Navarro and Sousa formations is oblate, with magnetic foliation (F) predominant over the magnetic lineation (L) (Figure 8f, also observed as positive T values on Table 1). Magnetic lineation (L) predominance is observed mainly close to the Western Malta Fault (WMF in Table 1), where the prolate ellipsoid shape is also highlighted by the negative T values (Table 1).

Hysteresis loops uniformly showed the superimposition of a prevailing linear paramagnetic component with wasp-waisted loops (Figures 7a and 7b). They can be associated with two magnetic components with strongly contrasting coercivities (Roberts et al., 1995), magnetite and hematite, as highlighted by the thermomagnetic curves (Figures 7c and 7d).

The magnetic fabric of the whole basin is characterized by NW-SE K_1 direction with vertical minimum magnetic susceptibility (K_3) after bedding correction (Figure 8a). The same pattern can be observed individually on both Sousa and Brejo das Freiras sub-basins (Figures 8b and 8c). However, the Gaussian-best-fit statistical analysis of the whole population of K_1 values ($n = 531$ data) indicates a bimodal distribution with two main distinct AMS fabrics (and stretching directions) in the whole basin: the main fabric with K_1 trending toward NW (N47°W with standard deviation of 30°), and a second one with K_1 trending toward NNE (N32°E with standard deviation of 27°) (Figure 8d, gray histogram). The results are similar if using data of sites presenting tectonic magnetic fabric ($n = 384$ data) with main fabric with K_1 trending toward NW (N48°W with standard deviation of 30°) and second fabric with K_1 trending toward NE (N28°E with standard deviation of 24°) (Figure 8d, white histogram). The corrected anisotropy degree and mean anisotropy degree of sites affected by tectonics is similar to those found in undisturbed sedimentary fabric, or non-tectonic fabric (Figure 8e). The same is observed in the relation magnetic lineation versus magnetic foliation (Figure 8f). A progressive change between the two main directions is inferred, as indicated by the non-well clustered data and the overlapped Gaussian-best-fit curves.

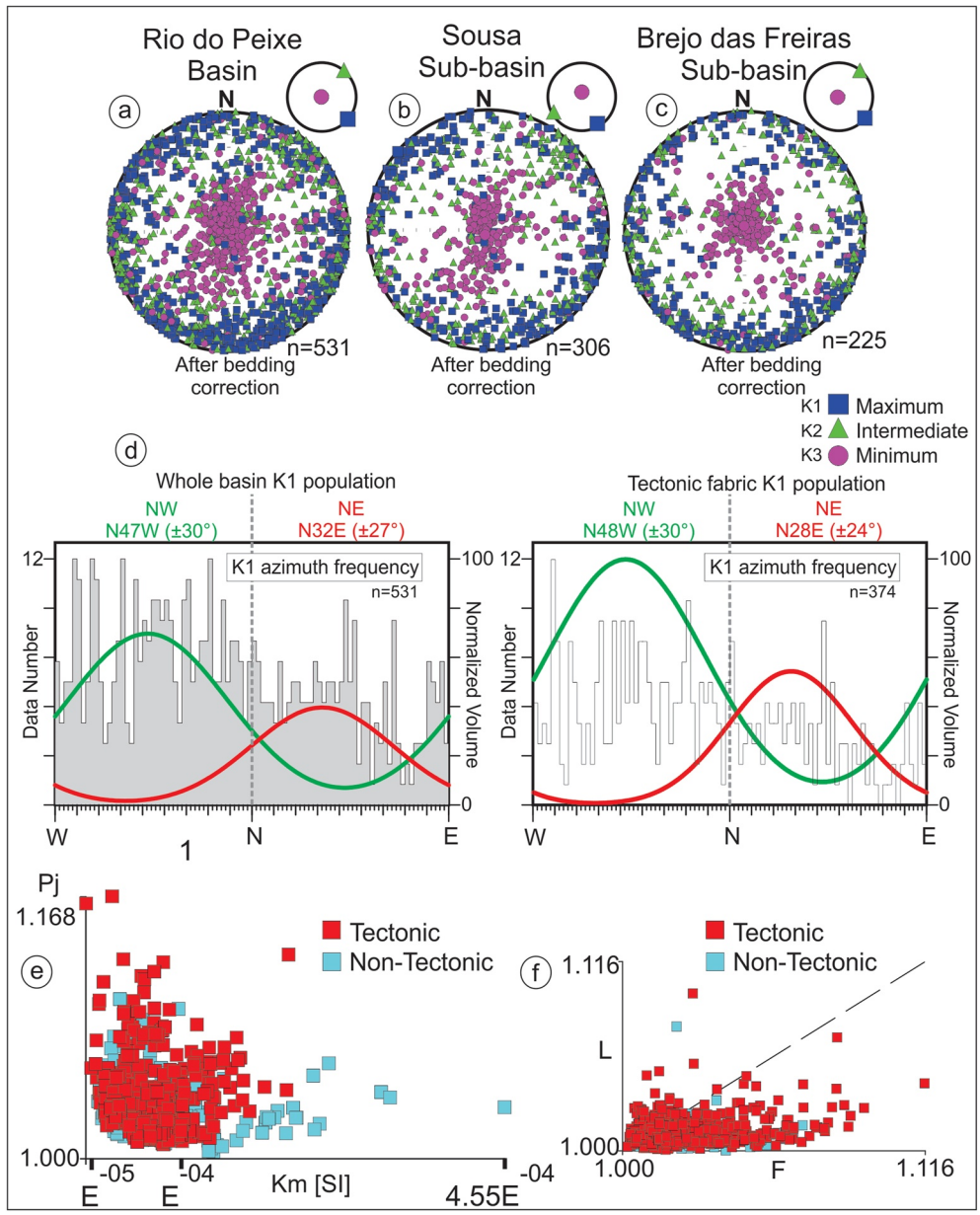

Figure 8. General AMS data. Stereonet with grouped values in the whole basin (a), Sousa Sub-basin (b) and Brejo das Freiras sub-basin (c). (d) Histogram with Gaussian-best-fit statistical analysis of the whole population of K_1 values (gray) and exclusively tectonic magnetic fabric (white). (e) Corrected anisotropy degree versus Mean anisotropy degree. (f) Magnetic lineation versus magnetic foliation. For E and F, samples with tectonic magnetic fabric are in red and samples with undisturbed sedimentary fabric are in blue.

4.3.2. AMS Fabric Along the Basin

Three distinct magnetic fabrics are observed in sedimentary units of the RPB, the non-tectonic fabric (formed due to sedimentary processes) (Figure 9), and the NNE and NW trending fabrics (formed due to tectonic processes) (Figures 8d and 10). Figure 10 depicts, for each sampling site, the mean orientation of K_1 using different color codes for different stretching directions. The non-tectonic fabric is found in samples collected on central zones of the Sousa sub-basin and close to the flexural border of the Brejo da Freiras sub-basin (i.e., along the whole western basin boundary zone). Additionally, non-tectonic magnetic fabric has also been found in samples collected close to the south Portalegre fault zone (Figure 10). In sites with non-tectonic magnetic fabric, the K_1 is distributed around the equatorial plane of stereonet (Figure 9a, sites SOC2 and UTND) or random orientation (Figure 9a,

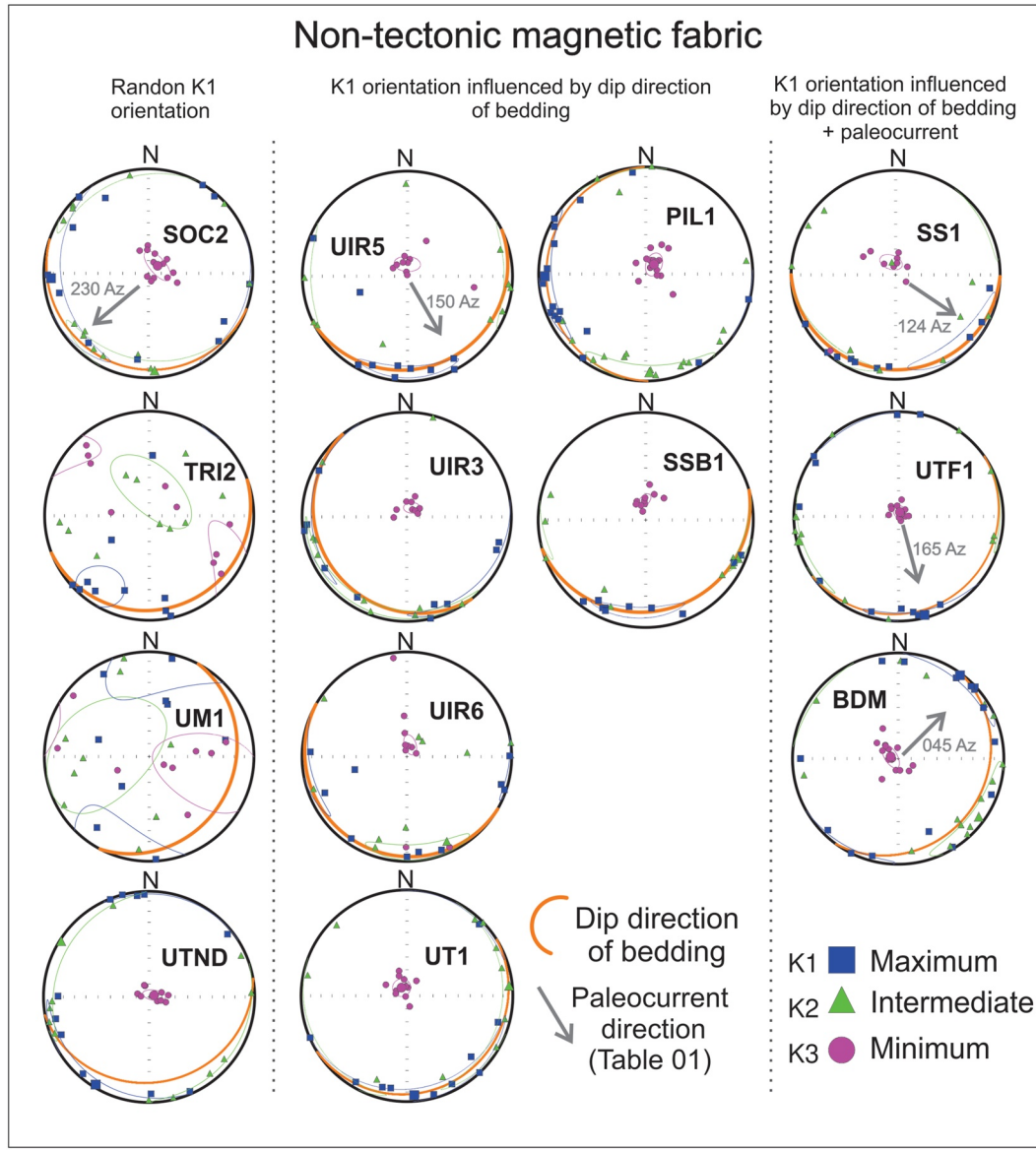

Figure 9. (a) Non-tectonic magnetic fabric with random orientation of K_1. (b) K_1 orientation influenced by the dip direction of bedding and (c) K_1 orientation influenced by the dip direction of bedding and the paleocurrent direction.

sites TRI2 and UM1) and/or distributed along the dip direction of bedding direction (Figure 9b) and/or oriented parallel to paleocurrent direction (Figure 9c).

The NNE-trending magnetic fabric presents low dispersion of K_1 orientation on stereogram is either N-S (sites UIR4F and CAV2) or NNE-oriented (sites PIL1, SES, MFW, MEL1, UIR4D, and SOC4) (Figure 10). The NNE-trending magnetic lineation is recorded mainly in sites at the contact zone between sedimentary units and crystalline basement or a few meters away from the border faults, either on Portalegre or Malta faults. This magnetic fabric occurs in the north (Figure 10, sites UIR4F and UIR4D) and south Portalegre Fault (sites CAV2, PIL2, and MEL1 in Figure 10). On the Eastern Malta Fault, the NNE-trending tectonic magnetic lineation is recorded in weakly deformed sediments located along the contact with the Malta Fault (e.g., site SOC4 in Figure 10). On the Western Malta Fault region, no clear K_1 NNE-direction was observed.

The NW-trending magnetic fabric generally presents low K_1 dispersion, with K_1 mostly oriented NW (sites UIR1-2, MEL2, CAVF, SB01, ASH12, VE1, VAR-2F, MARI2, and SOC3) and a few oriented WNW (sites DA123, MF1, and MARI3) (Figure 10). The NW-trending K_1 is dominant in the inner regions of the basin and

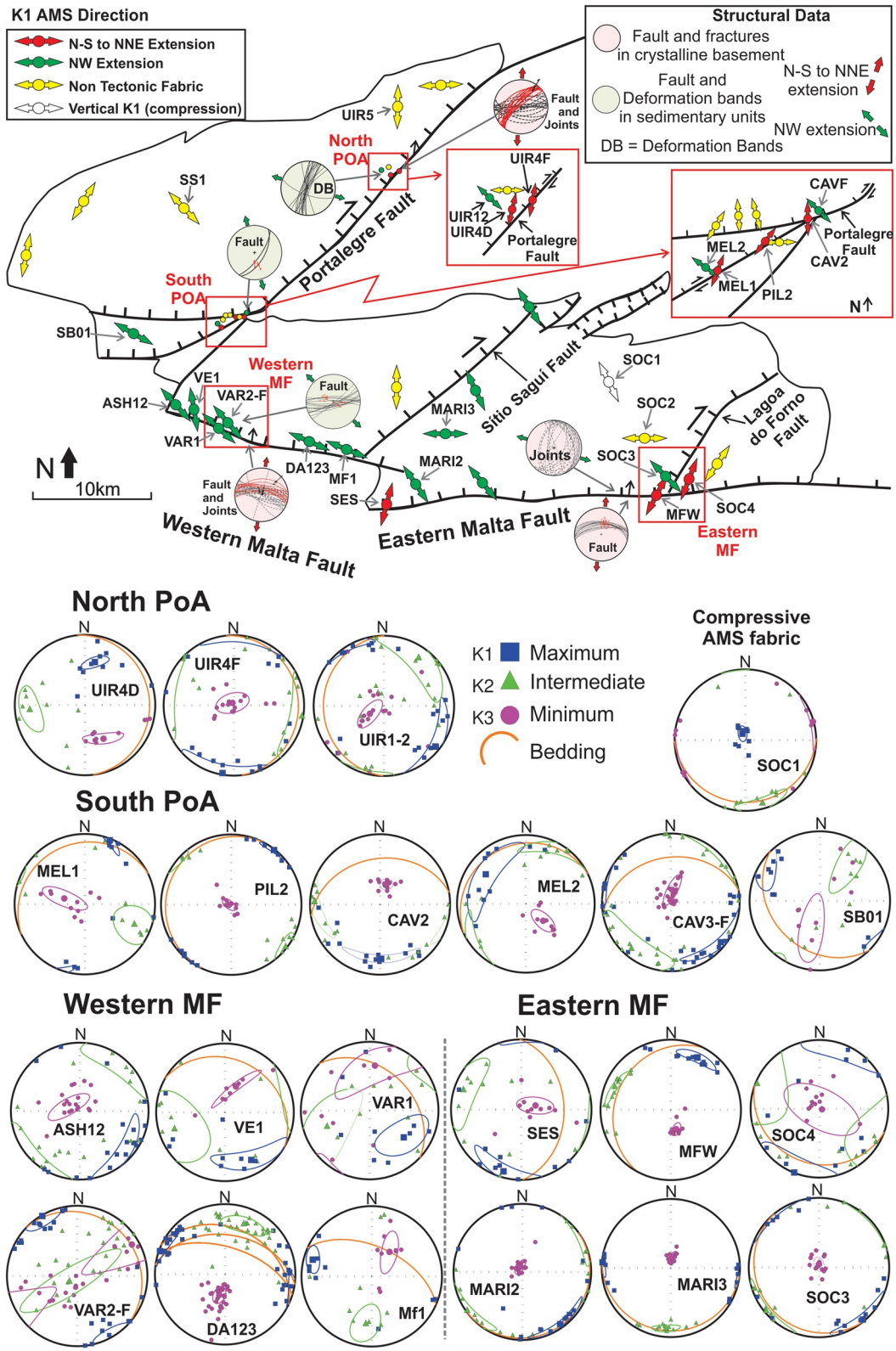

Figure 10.

also close to fault zones (Figure 10). Close to the border faults, the NW-trending K_1 is observed mostly on sites collected in the hangingwall damage zone, where NE-trending structures (minor faults and/or deformation bands) are present (Figures 4d and 5, South Portalegre Fault and Western Malta Fault, respectively). In the northern Portalegre Fault, the NW-trending K_1 was found several meters away from the main fault surface (Figure 10, site UIR12), where low deformation is observed due to the presence of NNE-trending deformation bands (Figure 3c and 3d). The same AMS fabric is observed in the Southern Portalegre Fault on both deformed zones (Figure 10, sites CAVF and MEL2) and on apparently non-deformed outcrops (SB01 in Figure 10). Along the Western Malta Fault (VAR2-F, DA123, and MF1 on Figure 10), the NW-trending K_1 is predominant very close to the border fault, where the rock is constantly affected by ~NE-striking extensional faults and deformation bands in sedimentary units. At the Eastern Malta Fault segment, the NW-trending K_1 is observed at the western part of the fault (MARI1 and MARI2 in Figure 10). At the easternmost region of the East Malta Fault, the NW-trending K_1 is well marked in the inner zone of the basin, mostly where the Lagoa do Forno Fault is probably influential (SOC3 in Figure 10).

5. Discussions

5.1. Magnetic Fabric of the Rio do Peixe Basin

The magnetic fabric (AMS) of the RPB may provide important information about the tectonic opening of the basin, as the main magnetic susceptibility (K_1) direction tend to be parallel to the stretching direction in sedimentary basins (e.g., Cifelli et al., 2004; Lanza & Meloni, 2006; Rochette et al., 1992). The dating available in the bibliography yielded Cretaceous ages (Arai, 2006; Lima & Coelho, 1987; Sousa et al., 2018) for Sousa, Antenor Navarro and Rio Piranhas formations. Therefore, it is not feasible to interpret the chronology of the magnetic fabrics based on dating. Based on the comparison between K axes, tectonic structures and paleocurrent directions in the study area, we interpret the acquired magnetic fabric as the result of tectonic deformation or sedimentary features of the rocks (Borradaile & Jackson, 2004; Lanza & Meloni, 2006). No correlation between geological formations and K_1 directions were observed, thus we interpret that the magnetic fabrics acquired in our samples represents either tectonic or undisturbed sedimentary fabric. Concerning the tectonic magnetic fabric, the Gaussian best-fit statistical analyses of all K_1 values (Figure 8d) indicate two main stretching directions responsible for the opening of the basin, that is, oriented ~N-S to NNE and ~NW. The N-S- to NNE-trending magnetic fabric (K_1) is limited to the contact zone between the crystalline basement and sedimentary units (i.e., in the fault damage zone affecting sedimentary units). It is concordant with the extensional direction inferred from brittle structures recorded in the crystalline basement rocks of both Portalegre and Malta border faults (joints and fault striae) (Figures 6 and 10). Conversely, the NW-trending magnetic fabric (K_1) is observed in the inner parts of the basin in apparently undeformed sandstones, and in the hangingwall damage zone sandstone of Portalegre and Malta border faults (Figure 10). The NW magnetic fabric is concordant with the extensional direction inferred from minor faults in sedimentary units (Figure 10).

The occurrence of two distinct, mutually orthogonal tectonic magnetic fabrics recorded in the syn-rift deposits concord with the extension directions (σ_3) inferred from structural data collected along the major border faults. It suggests that two main syn-rift phases were responsible for developing the RPB: an early N-S to NNE-SSW stretching direction (syn-rift I) followed by a NW-SE stretching direction (syn-rift II). The following lines of evidence support this relative chronology between the two stretching directions:

1. Structural data showing different extension directions in the crystalline basement and sedimentary units (Figure 10). The footwall damage zone of Malta and Portalegre border faults (i.e., in the crystalline basement rocks) show an extension direction (σ3) invariably oriented N-S to NNE-SSW. In contrast, in the sedimentary rocks, the NW-trending direction is dominant in the inner portions of the basin and along the Malta and Portalegre faults. The general lack of minor faults and deformation bands with a NW-trending extension in the hangingwall damage zone of the Malta Fault indicated that, in the first stage of tectonic opening of the basin, the mylonitic foliations in the basement were reactivated under a N-S to NNE-SSW stretching directions.

Figure 10. Map of Rio do Peixe Basin with K_1 direction of sampling sites and stereonet of the samples collected close to the main border faults. Red arrows indicate N-S to NNE-SSW K_1 direction and extension. Green arrows indicate NW-SE K_1 direction and extension. Yellow arrows indicate K_1 direction of samples with non-tectonic magnetic fabric (i.e., magnetic fabric influenced by the dip direction of bedding and/or the paleocurrent). The white arrow indicates vertical K_1 direction with the arrow pointing toward K_2. North POA = North Portalegre Fault. South POA = South Portalegre Fault. Western MF = Western Malta Fault. Eastern MF = Eastern Malta Fault.

This extension was responsible for the normal and transtensive kinematics of the Malta and Portalegre fault, respectively. Subsequently, after further sediment infilling, the stretching direction turned into NW-SE-trending. This is confirmed by the widespread NW-trending σ3, inferred from NE-striking extensional faults and deformation bands in the sedimentary rocks. The opposite relative chronology, that is, a late-stage N-S stretching, would have produced subsidiary structures in the hangingwall damage zones indicating N-S extension direction, which are completely lacking along the Malta Fault.

2. The Gaussian-best fit statistical analysis of K_1 values (Figure 8d) shows bimodal distribution with predominant NW-oriented data, suggesting that this stretching direction was probably more intense and also younger and likely acted in a longer period than the other stretching direction.
3. The cross-cutting relationship between deformation bands and quartz veins in the northern Portalegre Fault indicates that mm-thick quartz veins reopened the NNE-SSW deformation bands (Figure 3d). It suggests a late-stage reactivation of previous structures developed during the right-lateral strike-slip transtension under a NW-SE-trending stretching direction.
4. The NE-striking open fractures cross-cutting the E-W-striking Eastern Malta Fault (Figure 6c) also support the interpretation that the NW-SE extension occurs as a second stretching direction during the development of the basin.

We also identified a tectonic magnetic fabric mostly far from border faults (with scattered K_3 around the equatorial plane of stereonets) and a vertical magnetic lineation in only one site (SOC01). Although this magnetic fabric could indicate a compressive stress field responsible for basin inversion (Nogueira et al., 2015; Vasconcelos et al., 2021), our AMS data are not conclusive in discussing the post-rift inversion stage. Additionally, subsurface data suggest that inverted faults within the basin are not sufficiently developed to reach the surface (Vasconcelos et al., 2021). Thus, it indicates that the basin inversion might not be strong enough to change the previously formed magnetic fabric of sedimentary units, thus justifying the lack of compressive magnetic fabrics and related meso-structural evidence along the basin.

5.2. The N-S to NNE Extensional Tectonics of the Rio do Peixe Basin

The N-S to NNE stretching direction represents the early tectonic stage of the RPB, that is, the syn-rift phase I (Figure 10a). In this stage, the E-W-striking mylonitic foliation acted as a weakness zone that facilitated the brittle reactivation of the Patos ductile shear zone, forming the E-W-trending Malta fault (de Castro et al., 2007; Françolin et al., 1994; Nogueira et al., 2015). During this stage, the N-S to NNE extension resulted in dextral transtensive reactivation of the NE-striking Portalegre Fault in its northernmost region. The normal to oblique displacement at its southernmost region fault interacted with E-W fault trends forming "horsetail" fault tip geometry (Vasconcelos et al., 2021). The same stretching direction resulted in the early opening of the SSB, forming the E-W striking normal faults dipping toward the north, facilitated by the ductile foliation of the E-W-striking Patos Shear Zone. In the Western Malta Fault, the block movement toward the north affected the former NE-striking ductile shear zones, developing the Sitio Saguí fault with dextral transtensive kinematics (Figure 11a). The N-S to NNE extension on the Eastern Malta Fault resulted in normal faulting with down-dip striae toward the north, developing the Lagoa do Forno Fault as a right-lateral transtensive structure. Although the intrabasinal NE-striking faults are blind, seismic data show that both faults occur as negative flower structures (Vasconcelos et al., 2021), strengthening our interpretation. In summary, the early syn-rift brittle faulting followed the former sigmoidal ductile foliation geometry of the basement, imparted by the Portalegre (NE-trending) and Patos (E-W-trending) shear zones, dictating the actual geometry of the Rio do Peixe Basin.

5.3. The NW Extensional Tectonics of the Rio do Peixe Basin

The NW extension represents the syn-rift phase II of the Rio do Peixe Basin (Figure 11b). This stretching direction, corresponding to the most representative AMS fabric, reactivated the former NE-striking faults in a normal shear sense, as the stretching direction is orthogonal to the favorably oriented fault surfaces. This extensional reactivation is observed in the Portalegre Fault (Figure 11b) and at subsurface in the Sitio Saguí and Lagoa do Forno faults (Vasconcelos et al., 2021) (Figure 11b). As the NW-SE extension became dominant, the E-W- Malta and E-W-striking south Portalegre faults were reactivated on a left-lateral transtensional sense, as documented by structural data (minor faults and deformation bands) in these sites (Figures 5c and 5d). The deformation occurs mostly on coarse sandstone units at the inflection zones of the Portalegre fault zone, reflecting the deep fault reactivation (Araujo et al., 2018). In the BFSB, the faults occur as synthetic and antithetic structures from the basin boundary Portalegre Fault. In the SSB, the deformation is observed at its westernmost region, where NE-striking

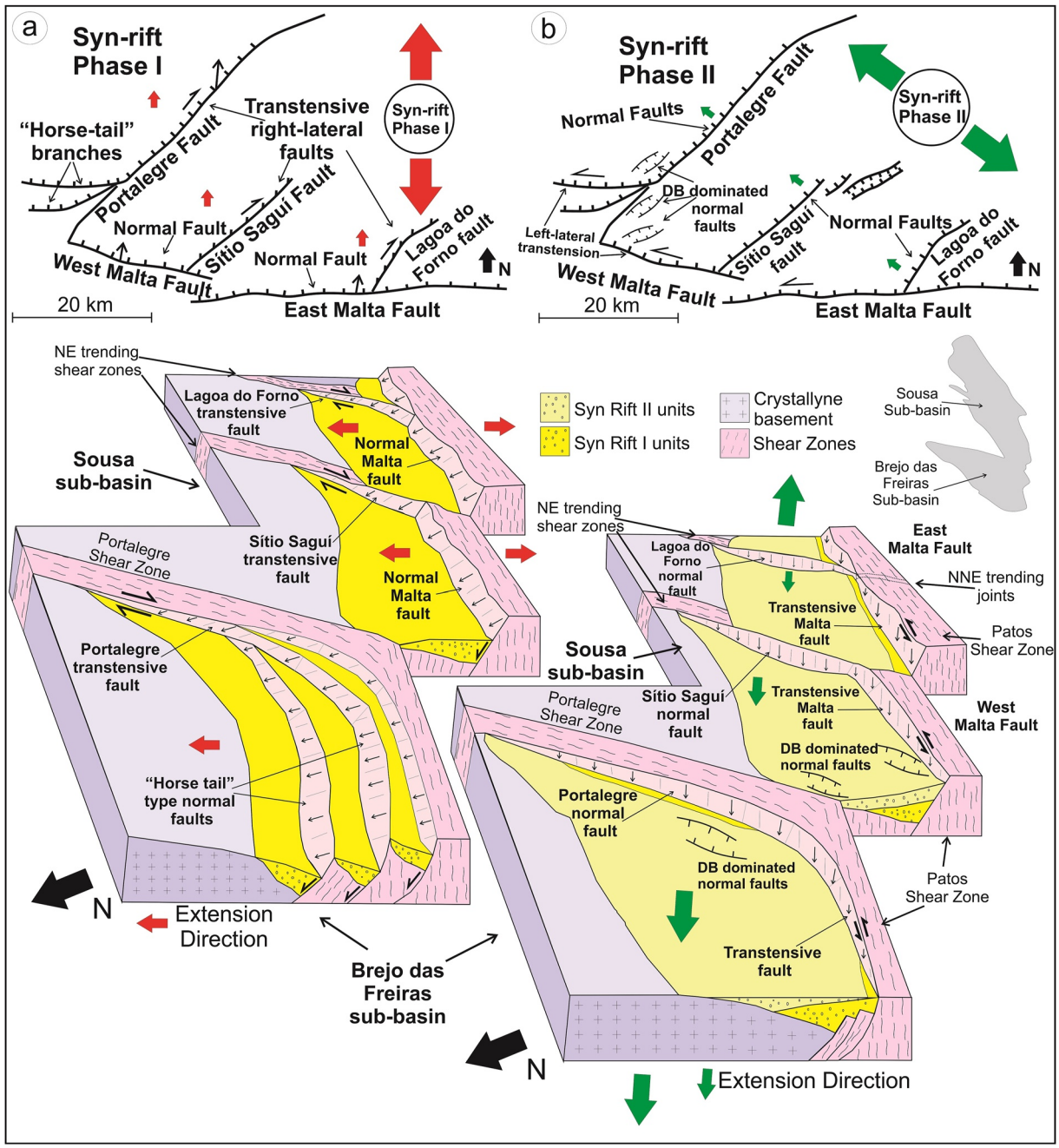

Figure 11. Schematic model of the syn-rift phase I and II in the Rio do Peixe Basin. (a) Syn-rift phase (i) The red arrows indicate the N-S- to NNE-oriented extension forming the E-W-striking Malta Fault, with normal kinematics and dipping to the north. Consequently, it resulted in right-lateral transtensive faults along the NE-striking Portalegre and other NE-striking faults. They are from, W to E, the Portalegre, Sítio Saguí, and Lagoa do Forno faults. (b) Syn-rift phase II. The green arrows indicate NW-oriented extension. It resulted in the reactivation of the NE-striking Portalegre, Sitio Saguí, and Lagoa do Forno faults. The kinematics had a normal shear sense, dipping to NW and consequently reactivating the E-W-striking Malta fault in a left-lateral transtensive sense. Extensional NE-striking faults and deformation bands (DB) were formed within the basin.

normal to left-lateral transtensive faults in sediments occurs obliquely from the East Malta E-W-striking Fault. NW extension is barely observed on the West Malta Fault, forming a few NE-striking deformation bands and NNE-trending joints perpendicularly cross-cutting the E-W-striking Malta Fault.

The presence of two distinct Gaussian best-fit curves, characterized by broad standard deviations and partial overlap (Figure 8d), suggest that the change in the stretching direction from NNE to NW was progressive in time and did not occurred in two disting tectonic events. This interpretation of progressive rotation of stretching direction

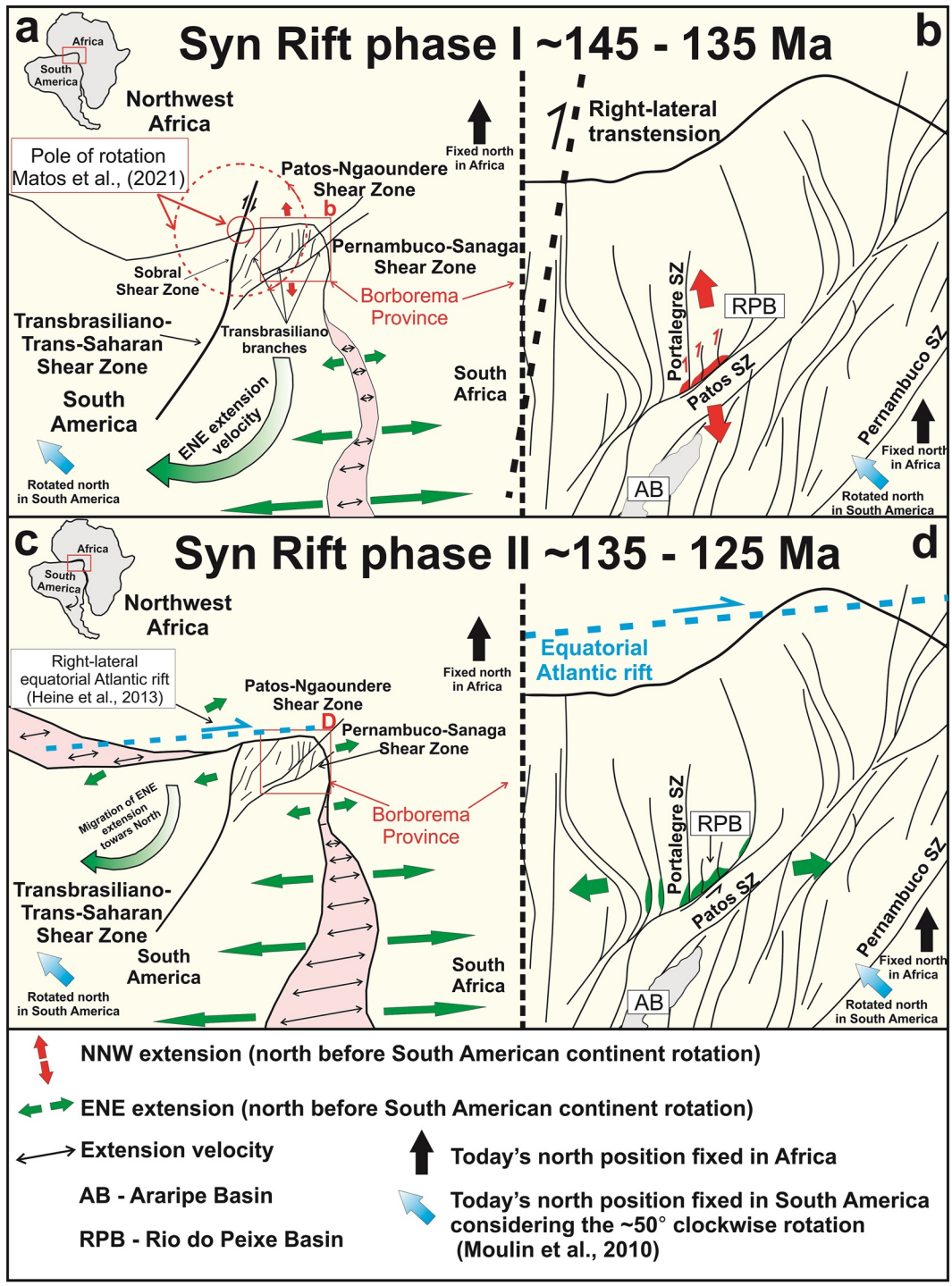

Figure 12.

is in good agreement with our fault slip data and is also consistent with the gradual clockwise stress rotation in northeast Brazil before the Pangea Breakup (cf. Matos et al., 2021).

5.4. Rio do Peixe Basin Rifting and Implications for the Pangea Breakup

The rifting of the Rio do Peixe Basin is related to the opening of the Atlantic Ocean (Matos, 1992). Therefore, to understand the development of the basin in the framework of plate tectonics, it is important to return to the pre-Pangea breakup configuration (Figure 12). In this pre-basin period, the South American continent was still

welded to West Africa, and the intraplate deformation was dominant in NE Brazil (de Castro et al., 2007; Moulin et al., 2010; Matos et al., 2021; Torsvik et al., 2009). Before the Pangea breakup, the South American continent was subjected to a clockwise stress rotation. Although the angle of such rotation is not clear after the pre-breakup interval, considering today's geographic position, the total continent rotation reached up to 40°–50° concerning West Africa (Moulin et al., 2010). Therefore, when this rotation was applied, the two stretching directions acting during the rifting phase were oriented ~NNW-SSE (syn-rift I; N32°E – 45°) and ~E-W (syn-rift II, N47°W–45°), respectively. It is essential to make clear that during the opening of the South Atlantic, South America underwent very minor rotation concerning Earth's spin axis and therefore respect to the cardinal points, while Africa underwent a much larger rotation (Somoza & Zaffarana, 2008). Therefore, the rotation of South America with respect to Africa used in this study is a relative rotation between two plates and should not be understood as a rotation relative to the global geographic coordinates, but just hypothetically assumed in a geographic frame that keeps Africa fixed in present-day coordinates.

Considering the actual geographic position of the South American continent, the N-S extension during the pre-breakup of Pangea was documented by several studies focused on plate reconstruction (Eagles & König, 2008; Heine et al., 2013; Moulin et al., 2010; Torsvik et al., 2009). This stretching direction was likely caused by the clockwise rotation of the South American continent concerning Africa during the Cretaceous (Françolin et al., 1994; Matos, 1992; Matos et al., 2021), with the regional pole of rotation located at the junction of the Transbrasiliano and the Trans-Saharan lineaments (Matos et al., 2021). Thus, when the RPB started developing (145 Ma) (Nóbrega et al., 2004), the Patos and Portalegre shear zones were oriented NE and N-S, respectively (Figure 12).

Matos et al. (2021) subdivided the South Atlantic Cretaceous Rift System into six distinct structural segments, including the Rio do Peixe Basin in the Cariri Rift Valley, affected by the NNW-SSE extension of the orthogonal branch. This zone was affected by dextral oblique-slip kinematics that lasted until the Barremian (Nóbrega et al., 2004; Matos et al., 2021) accommodated along the Transbrasiliano shear zone (Almeida et al., 2000) (Figure 12a). The NNW-SSE extension in the Rio do Peixe Basin area would be the result of the right-lateral strike-slip motion of the NNE-trending continental ductile shear zones. It matches with our NNE-oriented extension of syn-rift phase I data (Figure 12b) once the continent rotation of ~45° is considered (Moulin et al., 2010). As the Lower Cretaceous rift developed, the E-W-oriented σ3 was associated with the South Atlantic opening and continuously migrated toward the north (Eagles, 2007) up to the Rio do Peixe Basin, thus progressively becoming the dominant stretching direction in this stage (Figure 12c). As the E-W extension occurred with higher velocities at the southern part of the South Atlantic, the South American Plate was forced to rotate clockwise (Heine et al., 2013), thus gradually increasing the contribution of the E-W-oriented extension in the Borborema Province, changing the stress field in the Rio do Peixe Basin and further reactivating the basin-boundary Portalegre and Malta faults (Figures 12a and 12c). The forced continent rotation resulted in gradual normal stress-field rotation from NNW-SSE to E-W (cf. Heine et al., 2013). The overlap of K_1 data distribution (Figure 7) allows us to infer that the rotation in the stretching directions is progressive rather than a sudden switch imparted by two distinct syn-rift tectonic stages.

The exact age when the E-W-oriented extension became stronger than the NNW extension at Rio do Peixe Basin is unclear, as geochronological data is scarce in the Rio do Peixe basin. However, Matos et al. (2021) used the Mesozoic Equatorial Atlantic Magmatic Province (EQUAMP) (Hollanda et al., 2019), which they called Borborema Giant Dyke, to control the rifting age in the whole Borborema Province. In the RPB area, this event

Figure 12. Schematic model of the Pangea breakup with emphasis on the Borborema Province and Rio do Peixe Basin with north rotated anticlockwise considering the geographic north position in South America during the pre-breakup (modified from Moulin et al., 2010). (a) Syn-rift phase I scheme during the initial rotational stress in the South American continent. The ENE-oriented extension started the breakup in the south of the South American continent, with stretching intensity gradually migrating northwards. In the Borborema Province, the rotation of the stress field generated a right-lateral transtension along the Transbrasiliano-Trans-Saharan shear zones with the pole of rotation at their intersection (Matos et al., 2021). It resulted in the NNW-oriented distension in Transbrasiliano Shear Zone branches such as the NE-trending Patos Shear Zone (E-W-striking today and NE-striking on the Cretaceous north position in the South American continent, considering the ±50° clockwise rotation after continent spreading), and the opening of the Rio do Peixe Basin (b). Although studies of paleographic reconstructions between North America South and Africa point out that South America was at the same latitudes as today (e.g., Somoza & Zaffarana, 2008), the rotation of South America with respect to Africa used in this figure is a relative rotation between two plates and not a rotation relative to the global geographic coordinates. Thus, all cardinal points indicated in this figure assume that Africa is fixed in global coordinates. (c) Syn-rift phase II scheme. The development of the South Atlantic opening gradually increased the intensity of the ENE extension toward the north, arriving in the Borborema Province. (d) The arrival of the ENE stretching at the Borborema Province resulted in the reactivation of the N-S faults in Rio do Peixe Basin, changing the main stretching direction to the ENE trend. On today's north position, N-S structures became NE-striking, and NE structures became E-W-striking.

is roughly NE-oriented, suggesting a NW-SE-oriented extension (in today's north position and ~E-W-oriented extension in Pre-Pangea Breakup north position). The age of this event is 135–120 Ma. Thus, in our model (Figures 12c and 12d), we interpret that the ~E-W-oriented extension became the most influent in the Rio do Peixe Basin between 135 and 125 Ma, as the intraplate deformation has ceased at the Aptian-Albian boundary ~120 Ma (Heine et al., 2013; Moulin et al., 2010).

6. Conclusions

This study combined AMS and structural data to interpret the strain trajectories responsible for opening the Rio do Peixe Basin. Our data show that two distinct main stretching directions, diverging at about 80°, occurred during rifting. The stretching direction gradually rotated counterclockwise from NNE-SSW to NW-SE due to the intraplate stress rotations in a pre-Pangea breakup period.

The NNE-SSW-oriented stretching controlled the syn-rift phase I, marking the initial opening stage of the basin during the Berriasian. This extension resulted in the right-lateral displacement of the Transbrasiliano-Trans-Saharian shear zones. In the SSB, this phase caused the initial brittle deformation on the normal Malta Fault, striking E-W and dipping to the north. Due to block movement toward the north, the right-lateral transtensive NE-striking Sítio Saguí and Lagoa do Forno faults were formed, facilitated by former NE-striking Precambrian shear zones. The deformational pattern was repeated in the BFSB, with E-W inflection of the Portalegre Fault. It opened as a normal fault with hangingwall movement toward the north, resulting in right-lateral transtensive displacement of the NE-striking Portalegre Fault.

The NW-SE-oriented stretching was associated with the syn-rift phase II. It marked the increase of intensity of the E-W extension (considering the pre-continent rotation north) on northeast Brazil and West Africa that gradually migrated northwards during the opening of the South Atlantic. In the Rio do Peixe Basin, this stretching direction lasted from the Barremian to late Aptian, when the continent breakup started at the northern part of the Borborema Province, Brazil. During the syn-rift phase II of the basin, NE-trending faults assumed major relevance, reactivating in a normal sense. The new block movement direction resulted in left-lateral transtension of the E-W-striking border faults. This pattern was repeated on both Sousa and Brejo das Freiras sub-basins. NE-striking extensional faults were formed in the basin, reflecting the deep fault reactivation. Our results indicate that integrating structural and AMS data can be used for tectonic reconstructions and to infer the progressive evolution of the strain in intraplate settings. This approach opens new research lines to understand better the tectonic evolution of intraplate basins in NE Brazil.

Data Availability Statement

The AMS data used in this work are available in the Mendeley Data Repository (https://data.mendeley.com/drafts/zmsbs88kww) DOI: https://doi.org/10.17632/zmsbs88kww.1.

Acknowledgments
We acknowledge the associate editor Agusto Rapalini, Pablo Calvín and another anonymous reviewer for their thorough manuscript revisions. We are grateful to the Brazilian Oil Company Petrobras that funded the DEBRIP Project (TC 5850.0109438.18.9) coordinated by Francisco C. C. Nogueira (UFCG). We also acknowledge Aldo Winkler for helping in hysteresis loops measurements at INGV in Rome. Open Access Funding provided by Universita degli Studi di Parma within the CRUI–CARE Agreement.

References

Almeida, F. F. M. D., Neves, B., De, B. B., & Dal Ré Carneiro, C. (2000). The origin and evolution of the South American platform. *Earth-Science Reviews*, *50*(1–2), 77–111. https://doi.org/10.1016/S0012-8252(99)00072-0

Arai, M. (2006). Revisão estratigráfica do Cretáceo inferior das bacias interiores do Nordeste do Brasil. *Geociencias*, *25*(1), 7–15.

Araujo, R. E. B., Bezerra, F. H. R., Nogueira, F. C. C., Balsamo, F., Carvalho, B. R. B. M., Souza, J. A. B., et al. (2018). Basement control on fault formation and deformation band damage zone evolution in the Rio do Peixe Basin, Brazil. *Tectonophysics*, *745*(August), 117–131. https://doi.org/10.1016/j.tecto.2018.08.011

Borradaile, G. J. (1988). Magnetic susceptibility, petrofabrics and strain. *Tectonophysics*, *156*, 1–20. https://doi.org/10.1016/0040-1951(88)90279-x

Borradaile, G. J., & Jackson, M. (2004). Ams: Magnetic petrofabrics of deformed rocks.

Borradaile, G. J., & Tarling, D. (1981). The influence of deformation mechanisms on magnetic fabrics in waekly deformed rocks. *Tectonophysics*, *77*, 151–168. https://doi.org/10.1016/0040-1951(81)90165-7

Celestino, M. A. L., Miranda, T. S. D., Mariano, G., Alencar, M. D. L., Carvalho, B. R. B. M. D., Falcão, T. D. C., et al. (2020). Fault damage zones width: Implications for the tectonic evolution of the northern border of the Araripe Basin, Brazil, NE Brazil. *Journal of Structural Geology*, *138*(June). https://doi.org/10.1016/j.jsg.2020.104116

Chadima, M., & Jelinek, V. (2009). *Anisoft 4.2: Anisotropy data Browser for Windows*. Agico, Inc.

Cifelli, F., Mattei, M., Chadima, M., Hirt, A. M., & Hansen, A. (2005). The origin of tectonic lineation in extensional basins: Combined neutron texture and magnetic analyses on "undeformed" clays. *Earth and Planetary Science Letters*, *235*(1–2), 62–78. https://doi.org/10.1016/j.epsl.2005.02.042

Cifelli, F., Rossetti, F., Mattei, M., Hirt, A. M., Funiciello, R., & Tortorici, L. (2004). An AMS, structural and paleomagnetic study of quaternary deformation in eastern Sicily. *Journal of Structural Geology*, *26*(1), 29–46. https://doi.org/10.1016/S0191-8141(03)00092-0

Da Nóbrega, M. A., Sá, J. M., Bezerra, F. H. R., Hadler Neto, J. C., Iunes, P. J., Guedes, S., et al. (2005). The use of apatite fission track thermochronology to constrain fault movements and sedimentary basin evolution in northeastern Brazil. *Radiation Measurements*, *39*(6), 627–633. https://doi.org/10.1016/j.radmeas.2004.12.006

De Castro, D. L., De Oliveira, D. C., & Gomes Castelo Branco, R. M. (2007). On the tectonics of the Neocomian Rio do Peixe Rift Basin, NE Brazil: Lessons from gravity, magnetics, and radiometric data. *Journal of South American Earth Sciences*, *24*(2–4), 184–202. https://doi.org/10.1016/j.jsames.2007.04.001

Dyer, R. (1988). Using joint interactions to estimate paleostress ratios. *Journal of Structural Geology*, *10*(7), 685–699. https://doi.org/10.1016/0191-8141(88)90076-4

Eagles, G. (2007). New angles on South Atlantic opening. *Geophysical Journal International*, *168*(1), 353–361. https://doi.org/10.1111/j.1365-246X.2006.03206.x

Eagles, G., & König, M. (2008). A model of plate kinematics in gondwana breakup. *Geophysical Journal International*, *173*(2), 703–717. https://doi.org/10.1111/j.1365-246X.2008.03753.x

Faccenna, C., Speranza, F., Caracciolo, F. D. A., Mattei, M., & Oggiano, G. (2002). Extensional tectonics on Sardinia (Italy): Insights into the arc-back-arc transitional regime. *Tectonophysics*, *356*(4), 213–232. https://doi.org/10.1016/S0040-1951(02)00287-1

Françolin, J. B. L., Cobbold, P. R., & Szatmari, P. (1994). Faulting in the early cretaceous Rio do Peixe Basin (NE Brazil) and its significance for the opening of the Atlantic, *16*(5), 647–661.

Frizon De Lamotte, D., Fourdan, B., Leleu, S., Leparmentier, F., & De Clarens, P. (2015). Style of rifting and the stages of Pangea breakup. *Tectonics*, *34*(5), 1009–1029. https://doi.org/10.1002/2014TC003760

García-Lasanta, C., Oliva-Urcia, B., Casas-Sainz, A. M., Román-Berdiel, T., Izquierdo-Llavall, E., Soto, R., et al. (2018). Inversion tectonics and magnetic fabrics in mesozoic basins of the Western Tethys: A review. *Tectonophysics*, *745*(August), 1–23. https://doi.org/10.1016/j.tecto.2018.08.005

Gomes, C. P., Fossen, H., De Almeida, R. P., & Salmoni, B. (2018). Subseismic deformation in the Vaza-Barris Transfer zone in the cretaceous Recôncavo-Tucano-Jatobá Rift System, NE Brazil. *Journal of Structural Geology*, *117*(May), 81–95. https://doi.org/10.1016/j.jsg.2018.09.007

Hamilton, N., & Rees, A. I. (1970). The use of magnetic fabric in paleocurrent estimation. In S. K. Runcorn (Ed.), *Paleogeophysics* (pp. 445–464). Academic Press.

Heine, C., Zoethout, J., & Müller, R. D. (2013). Kinematics of the south Atlantic rift. *Solid Earth*, *4*(2), 215–253. https://doi.org/10.5194/se-4-215-2013

Hollanda, M. H. B. M., Archanjo, C. J., Macedo Filho, A. A., Fossen, H., Ernst, R. E., Castro, D. L. D., et al. (2019). The mesozoic equatorial atlantic magmatic province (EQUAMP). A new large igneous province in South America. In *Book: Dyke Swarms of the World: A modern Perspective*. https://doi.org/10.1007/978-981-13-1666-1_3

Hrouda, F. (1982). Magnetic anisotropy of rocks and its application in geology and geophysics. *Geophysical Surveys*, *5*, 37–82. https://doi.org/10.1007/BF01450244

Jelinek, V. (1981). Characterization of the magnetic fabric of rocks. *Tectonophysics*, *79*(3–4), 63–67. https://doi.org/10.1016/0040-1951(81)90110-4

Lanza, R., & Meloni, A. (2006). *The Earth's Magnetism. An introduction for geologists*. Springer.

Lee, T.-Q., Kissel, C., & Laj, C., & Chorng-Shern Horng, & Yi-The Lue. (1990). Magnetic fabric analysis of the Plio-Pleistocene sedimentary formations of the coastal range of Taiwan. *Earth and Planetary Science Letters*, *98*(1), 23–32. https://doi.org/10.1016/0012-821X(90)90085-C

Lima, M. R., & Coelho, P. C. (1987). Estudo palinológico da sondagem estratigráfica de Lagoa do Forno, Bacia do Rio do Peixe, Cretáceo do Nordeste do Brasil. *Bol. IG-USP, Sér. Cient., São-Paulo*, *18*, 67–85.

Lourenço, M. C. M., Jardim De Sá, E. F., Córdoba, V. C., & Pichel, L. M. (2021). Multi-scale tectono-stratigraphic analysis of pre- and syn-rift sequences in the Rio do Peixe Basin, NE Brazil. *Marine and Petroleum Geology*, *130*(May). https://doi.org/10.1016/j.marpetgeo.2021.105127

Maciel, I. B., Dettori, A., Balsamo, F., Bezerra, F. H. R., Vieira, M. M., Nogueira, F. C. C., et al. (2018). Structural control on clay mineral Authigenesis in faulted arkosic sandstone of the Rio do Peixe. *Minerals*, *8*, 17. https://doi.org/10.3390/min8090408

Marques, F. O., Nogueira, F. C. C., Bezerra, F. H. R., & De Castro, D. L. (2014). The Araripe basin in NE Brazil: An intracontinental graben inverted to a high-standing horst. *Tectonophysics*, *630*, 251–264.

Matos, R. M. D. (1992). The Northeast Brazilian Rift System. *Tectonics*, *11*(4), 766–791. https://doi.org/10.4324/9780203494219-10

Matos, R. M. D., Medeiros, W. E., Jardim de Sá, E. F., Almeida, C. B. D., Norton, I., & Córdoba, V. C. (2021). A solution to the Albian fit challenge between the South American and African plates based on key magmatic and sedimentary events late in the rifting phase in the Pernambuco and Paraíba basins. *Marine and Petroleum Geology*, *128*(September 2020). https://doi.org/10.1016/j.marpetgeo.2021.105038

Mattei, M., Sagnotti, L., Faccenna, C., & Funiciello, R. (1997). Magnetic fabric of weakly deformed clayey sediments in the Italian peninsula: Relationships with compressional and extensional tectonics. *Tectonophysics*, *271*, 107–122.

Moulin, M., Aslanian, D., & Unternehr, P. (2010). A new starting point for the south and equatorial Atlantic Ocean. *Earth-Science Reviews*, *98*(1–2), 1–37. https://doi.org/10.1016/j.earscirev.2009.08.001

Nicchio, M. A., Nogueira, F. C. C., Balsamo, F., Souza, J. A. B., Carvalho, B. R. B. M., & Bezerra, F. H. R. (2018). Development of cataclastic foliation in deformation bands in feldspar-rich conglomerates of the Rio do Peixe Basin, NE Brazil. *Journal of Structural Geology*, *107*(December 2017), 132–141. https://doi.org/10.1016/j.jsg.2017.12.013

Nogueira, F. C. C., De Castro, D. L., & De Oliveira, M. S. (2004). Estudo Magnético e Gravimétrico do Arcabouço Estrutural da Bacia Rio do Peixe - PB. *Revista de Geologia*, *17*(1), 74–87.

Nogueira, F. C. C., Marques, F. O., Bezerra, F. H. R., De Castro, D. L., & Fuck, R. A. (2015). Cretaceous intracontinental rifting and post-rift inversion in NE Brazil: Insights from the Rio do Peixe Basin. *Tectonophysics*, *644*, 92–107. https://doi.org/10.1016/j.tecto.2014.12.016

Nogueira, F. C. C., Nicchio, M. A., Balsamo, F., Souza, J. A. B., Silva, I. V. L., Bezerra, F. H. R., et al. (2021). The influence of the cataclastic matrix on the petrophysical properties of deformation bands in arkosic sandstones. *Marine and Petroleum Geology*, *124*(November), 15. https://doi.org/10.1016/j.marpetgeo.2020.104825

NogueiraCosta, F. C., Oliveira, M. S. De., & Castro, D. L. D. (2004). Estudo Magnético e Gravimétrico do Arcabouço Estrutural da Bacia Rio do Peixe – PB. *Revista de Geologia*, *17*(1), 74–87.

Oriolo, S., Oyhantçabal, P., Wemmer, K., & Siegesmund, S. (2017). Contemporaneous assembly of Western Gondwana and final Rodinia break-up: Implications for the supercontinent cycle. *Geoscience Frontiers*, *8*(6), 1431–1445. https://doi.org/10.1016/j.gsf.2017.01.009

Paterson, S. R., Yu, H., & Oertel, G. (1995). *Primary and tectonic fabric intensities in mudrocks*, *247*, 105–119.

Peace, A. L., Phethean, J. J. J., Franke, D., Foulger, G. R., Schiffer, C., Welford, J. K., et al. (2020). A review of Pangaea dispersal and Large Igneous Provinces – In search of a causative mechanism. *Earth-Science Reviews*, *206*(March), 102902. https://doi.org/10.1016/j.earscirev.2019.102902

Pontes, C. C. C., Nogueira, F. C. C., Bezerra, F. H. R., Balsamo, F., Miranda, T. S., Nicchio, M. A., et al. (2019). Petrophysical properties of deformation bands in high porous sandstones across fault zones in the Rio do Peixe Basin, Brazil. *International Journal of Rock Mechanics and Mining Sciences*, *114*(November 2018), 153–163. https://doi.org/10.1016/j.ijrmms.2018.12.009

Porreca, M., & Mattei, M. (2012). AMS fabric and tectonic evolution of Quaternary intramontane extensional basins in the Picentini Mountains (southern Apennines, Italy). *International Journal of Earth Sciences*, *101*(3), 863–877. https://doi.org/10.1007/s00531-011-0670-2

Rapozo, B. F., Córdoba, V. C., & Antunes, A. F. (2021). Tectono-stratigraphic evolution of a cretaceous intracontinental rift: Example from Rio do Peixe Basin, north-eastern Brazil. *Marine and Petroleum Geology*, *126*(January). https://doi.org/10.1016/j.marpetgeo.2021.104899

Roberts, A. P., Cui, Y., & Verosub, K.-L. (1995). Wasp-waisted hysteresis loops: Mineral magnetic characteristics and discrimination of components in mixed magnetic systems. *Journal of Geophysical Research: Solid EarthVolume*, *100*(B9), 17909–17924. https://doi.org/10.1029/95JB00672

Rochette, P., Jackson, M., & Aubourg, C. (1992). Rock magnetism and the interpretation of anisotropy of magnetic susceptibility. *Reviews of Geophysics*, *30*(3), 209–226.

Schwehr, K., & Tauxe, L. (2003). Characterization of soft-sediment deformation: Detection of cryptoslumps using magnetic methods. *Geology*, *31*(3), 203–206. https://doi.org/10.1130/0091-7613(2003)031<0203:COSSDD>2.0

Sénant, J., & Popoff, M. (1991). Early Cretaceous extension in northeast Brazil related to the South Atlantic opening. *Tectonophysics*, *198*(1), 35–46. https://doi.org/10.1016/0040-1951(91)90129-G

Silva, M. E., Nogueira, F. C. C., Pérez, Y. A. R., Vasconcelos, D. L., Stohler, R. C., & Sanglard, J. C. D. (2022). Permeability modeling of a basin-bounding fault damage zone in the Rio do Peixe Basin, Brazil. *Marine and Petroleum Geology*, *135*, 105409. https://doi.org/10.1016/j.marpetgeo.2021.105409

Somoza, R., & Zaffarana, C. B. (2008). Mid-Cretaceous polar standstill of South America, motion of the Atlantic hotspots and the birth of the Andean cordillera. *Earth and Planetary Science Letters*, *271*, 267–277. https://doi.org/10.1016/j.epsl.2008.04.004

Sousa, A. D. J. e., Carvalho, I. D. S., & Ferreira, E. P. (2018). Western Gondwana non-marine ostracods from Early Cretaceous low-latitude ephemeral lake, Northeastern Brazil. *Journal of South American Earth Sciences*, *86*(June), 23–37. https://doi.org/10.1016/j.jsames.2018.06.001

Souza, D. H. S., Nogueira, F. C. C., Vasconcelos, D. L., Torabi, A., Souza, J. A. B., Nicchio, M. A., et al. (2021). Growth of cataclastic bands into a Fault zone: A multiscalar process by microcrack coalescence in sandstones of Rio do Peixe basin, NE Brazil. *Journal of Structural Geology*, *146*(August 2020). https://doi.org/10.1016/j.jsg.2021.104315

Szatmari, P., Françolin, J. B. L., Zanotto, O., & Wolff, S. (1987). Evolução Tectônica Da Margem equatorial Brasileira. *Revista Brasileira de Geociencias*, *17*(2), 180–188. https://doi.org/10.25249/0375-7536.1987180188

Torabi, A., Balsamo, F., Nogueira, F. C. C., Vasconcelos, D. L., Silva, A. C. E., Bezerra, F. H. R., & Souza, J. A. B. (2021). Variation of thickness, internal structure and petrophysical properties in a deformation band fault zone in siliciclastic rocks. *Marine and Petroleum Geology*, *133*, 105297. https://doi.org/10.1016/j.marpetgeo.2021.105297

Torsvik, T. H., Rousse, S., Labails, C., & Smethurst, M. A. (2009). A new scheme for the opening of the South Atlantic Ocean and the dissection of an Aptian salt basin. *Geophysical Journal International*, *177*, 1315–1333. https://doi.org/10.1111/j.1365-246X.2009.04137.x

Vasconcelos, D. L., Marques, F. O., Nogueira, F. C. C., Perez, Y. A. R., Bezerra, F. H. R., Stohler, R. C., & Souza, J. A. B. (2021). Tectonic inversion assessed by integration of geological and geophysical data: The intracontinental Rio do Peixe Basin, NE Brazil. *Basin Research*, 1–24. (March). https://doi.org/10.1111/bre.12491